NACA

RESEARCH MEMORANDUM

INVESTIGATION OF A HIGH-PERFORMANCE AXIAL-FLOW COMPRESSOR TRANSONIC INLET ROTOR DESIGNED FOR 37.5 POUNDS PER SECOND PER SQUARE FOOT OF FRONTAL AREA

DETAILED BLADE-ELEMENT PERFORMANCE

By A. Richard Felix and Melvyn Savage

Langley Aeronautical Laboratory
Langley Field, Va.

WASHINGTON
April 12, 1957

Classification cancelled (or changed to Unclassified)

By Authority of Nat St Tech Pub Announcement #3
(OFFICER AUTHORIZED TO CHANGE)

By [illegible]
(NAME)

[illegible]
(GRADE OF OFFICER MAKING CHANGE)

[illegible]
DATE

NACA RM L56K23

NATIONAL ADVISORY COMMITTEE FOR AERONAUTICS

RESEARCH MEMORANDUM

INVESTIGATION OF A HIGH-PERFORMANCE AXIAL-FLOW COMPRESSOR TRANSONIC INLET ROTOR DESIGNED FOR 37.5 POUNDS PER SECOND PER SQUARE FOOT OF FRONTAL AREA

DETAILED BLADE-ELEMENT PERFORMANCE

By A. Richard Felix and Melvyn Savage

SUMMARY

Detailed blade-element-performance plots for a high-flow transonic inlet rotor have shown low losses at speeds up to 11 percent above design. Although the blade elements were set at angles of attack larger than the low-speed cascade design angles, the minimum losses occurred at still larger angles of attack. At 21 percent above design speed severe separation was noted near the tip where relative Mach numbers are of the order of 1.2. For all elements exclusive of the one nearest the tip the range of maximum values of static-pressure-rise coefficient for which minimum losses are low is quite narrow (from 0.45 to 0.48). The low-speed cascade data are fairly effective in the estimation of design turning angles at relative inlet Mach numbers as high as 1.06 for the main portion of the annulus which is free of flow separation and three-dimensional flow effects. A comparison between design and measured flow conditions indicates that better design control is desirable.

An examination of data for several other transonic rotors in the tip region indicates that for solidities from 0.78 to 1.32 and relative inlet Mach numbers near 1.0, the range of values of limiting static-pressure-rise coefficient is from 0.37 to 0.43. At a solidity of 0.66 the limiting value of static-pressure-rise coefficient at which losses increase rapidly is 0.315. Therefore, it appears desirable to avoid solidities much less than 0.75.

The shock-wave patterns in the tip region are shown by means of the shadowgraph technique.

INTRODUCTION

Detailed survey data have been obtained for the high-flow transonic inlet rotor whose overall performance characteristics were reported in reference 1. The purpose of the present paper is to present and analyze the blade-element performance of this rotor. The analysis includes the effects of Mach number, blade loading, and angle of attack on element performance. Also included are blade-loading data for several other transonic rotors.

SYMBOLS

A_f	frontal area, sq ft
c	blade chord, ft
c_{pm}	specific heat for Freon-air mixture at constant pressure obtained by using an average of upstream and downstream temperatures at each radial station
D	diffusion factor, $1 - \frac{V_{2R}}{V_{1R}} + \frac{\Delta V_{\theta R}}{2\sigma V_{1R}}$
w_e	equivalent weight flow, $w \frac{\sqrt{\theta}}{\delta}$, lb/sec
g	acceleration due to gravity
M	Mach number
N	rotor speed, rpm
p	static pressure, lb/sq ft
$\frac{\Delta p}{(P - p)_{1R}}$	static-pressure-rise coefficient, $\frac{p_2 - p_1}{(P - p)_{1R}}$
P	total pressure, lb/sq ft
r	radius, ft
w_e/A_f	specific weight flow, $w \frac{\sqrt{\theta}}{\delta A_f}$, lb/sec/sq ft

T	total temperature, $^{\circ}R$
ΔT	total temperature rise, $T_2 - T_1$, $^{\circ}R$
U	rotational speed, ft/sec
V	velocity, ft/sec
w	weight flow, lb/sec
α	angle of attack, angle between relative flow direction and blade chord, deg
$\Delta\alpha'$	difference between selected angle of attack and low-speed design angle of attack, $\alpha_s - \alpha_d$, deg
β	flow angle (between flow direction and axial direction), deg
δ	ratio of inlet total pressure to NACA standard sea-level total pressure of 2116.22 lb/sq ft
γ	ratio of specific heats
η_M	efficiency based on momentum
θ	ratio of inlet total temperature to NACA standard sea-level temperature of 518.688° R
θ_o	flow turning angle, $\beta_{1R} - \beta_{2R}$, deg
ρ	static density, slugs/cu ft
σ	solidity
$\bar{\omega}$	total pressure loss coefficient, $\frac{P_{1R} - P_{2R}}{(P - p)_{1R}}$

Subscripts:

A	air
a	axial
d	design
F	Freon

h	hub
isen	isentropic
min	minimum
R	relative to rotor blade
s	selected
θ	tangential
t	tip
1	upstream of rotor
2	downstream of rotor

ROTOR DESIGN CONDITIONS

The rotor design conditions in air are as follows:

Specific weight flow, w_e/A_f, lb/sec/sq ft	37.5
Mass-weighted total-pressure ratio, P_2/P_1	1.293
Tip speed, U_t, ft/sec	972
Inlet axial Mach number, M_{a1}	0.628
Inlet hub-tip ratio, r_{h1}/r_{t1}	0.35
Outlet hub-tip ratio, r_{h2}/r_{t2}	0.45
Tip radius, $r_{t1} = r_{t2}$, ft	0.500

The velocity-diagram data are presented in figure 1.

TEST PROCEDURE AND DATA REDUCTION

Test Procedure

The tests presented in this paper were made in a Freon atmosphere in the 3,000-hp compressor test stand at four speeds of $0.81N_d$, $1.00N_d$, $1.11N_d$, and $1.21N_d$ and a range of throttle settings from maximum flow to near surge. All speeds were corrected to standard temperature by multiplying by $\sqrt{\theta}$ where θ is the ratio of inlet total temperature to NACA standard sea-level temperature.

Data Reduction

The rotor design procedure, instrumentation, and data reduction have been reported in reference 1.

Surveys were made with a prism-type probe 1.5 inches upstream of the rotor at several weight flows. These surveys indicated a small amount of swirl (fig. 2), mostly at the tip, in the direction of rotation. Also, a slight gradient in static pressure was measured. All data presented herein have been recomputed from reference 1 data by using measured inlet swirl. As a result, blade-element efficiency η_M is computed from the following equation:

$$\eta_M = \frac{c_{pm}\,\Delta T_{isen}}{U_2 V_{\theta 2} - U_1 V_{\theta 1}}$$

where

$$\Delta T_{isen} = \left[\left(\frac{P_2}{P_1}\right)^{\frac{\gamma-1}{\gamma}} - 1\right] T_1$$

These efficiencies were mass weighted to obtain overall efficiencies.

RESULTS AND DISCUSSION

A motion-picture film supplement has been prepared in connection with the results discussed in the appendix and is available on loan. A request card form and a description of the film will be found at the back of this paper.

Overall Performance

The overall mass-weighted performance data are presented for the four speeds of $0.81N_d$, $1.00N_d$, $1.11N_d$, and $1.21N_d$ in figure 3. The dotted curves represent the momentum efficiency η_M, neglecting the inlet swirl as presented in reference 1. The efficiencies with inlet swirl included are approximately 3 percent higher than those without. The peak efficiency at $0.81N_d$ is approximately 0.93; at $1.00N_d$, 0.96; at $1.11N_d$, 0.91; and at $1.21N_d$, 0.87.

Blade-Element Performance

Description of a blade element.- The upstream annulus just ahead of the rotor was divided radially into 10 equal areas. Each of these 10 equal areas was divided into two equal areas, thus locating what is called an "equal-area center." The downstream annulus was treated in a similar manner, with the 10 downstream equal-area centers being located. Blade elements as used in this paper are those sections of the blade which lie on a conical surface connecting an upstream equal-area center with the corresponding downstream equal-area center. Figure 4 summarizes the equal-area-center calculated values. The computations of almost all blade-element characteristics were made for the 10 blade elements previously mentioned, but only five are used in the element plots of figure 5. These five elements are designated a, b, c, d, and e in figure 4.

Blade-element-performance parameters.- The flow turning angle θ_o, the total-pressure loss $\bar{\omega}$, and the momentum efficiency η_M are presented as three standard parameters for indicating blade-element performance. The effect of blade loading on the element performance is shown by including the parameters diffusion factor D and static-pressure-rise coefficient $\frac{\Delta p}{(P - p)_{1R}}$. The relative inlet Mach number M_{1R} and the axial velocity ratio V_{a2}/V_{a1} are included as parameters of interest in analyzing element losses. The total pressure ratio P_2/P_1 is also presented.

The blade-element plots show the variation of each of the aforementioned parameters $\bar{\omega}$, η_M, D, $\frac{\Delta p}{(P - p)_{1R}}$, M_{1R}, V_{a2}/V_{a1}, θ_o, and P_2/P_1 with angle of attack α for five blade elements, a, b, c, d, and e (figs. 5(a), 5(b), 5(c), 5(d), and 5(e), respectively).

Total-pressure loss.- At $0.81N_d$ and $1.00N_d$ the minimum total-pressure losses at all elements are in the low range of 0.06 or less. The minimum losses at $1.11N_d$ are also low with the exception of the loss at the tipmost element, e, which has a minimum loss of 0.14. The maximum relative inlet Mach number associated with these low-loss coefficients is 1.04. At $1.21N_d$ the increased loss region extends inward to element d. At this speed the minimum loss at element d is 0.10 and at element e is 0.25 and indicates a severe separation at the tip with accompanying Mach numbers at the two elements ranging from 1.08 to 1.22. Shadowgraphs of the shock-wave patterns in the tip region are discussed in the appendix.

The tendency for the minimum loss in a transonic rotor to occur at a higher angle of attack than in a low-speed rotor or in low-speed cascade was anticipated in the design of this rotor and lower-cambered sections at higher angles of attack were used. (See ref. 2.) These angles of attack, chosen to fulfill the design vector diagrams, are called selected angles of attack and are indicated by an arrow on each element plot in figure 5. The difference between the selected angle of attack and the low-speed cascade design angle of attack (ref. 3) is indicated on each element plot by $\Delta\alpha'$. The value of $\Delta\alpha'$ is based on the inlet flow angle of the design velocity diagram whereas the value of $\Delta\alpha$ indicated in figure 4 of reference 1 is based on the inlet flow angle corrected to mean axial velocity. The $\Delta\alpha'$ varies from 1.3° at element a to 2.7° at element e.

The angle of attack for minimum loss appears to be 3° to 4° larger than the selected angle of attack at element a, the element nearest the hub. This difference between the minimum-loss angle of attack and the selected angle of attack becomes less for the elements nearer the tip and at element e is approximately 0° to 1°. There is also a tendency, particularly noticeable at the more outboard elements, for the minimum-loss angle of attack to increase slightly as the speed is increased from $1.00N_d$ to $1.21N_d$.

The values given in the two preceding paragraphs indicate that the minimum loss at element a occurs at an angle approximately 4.3° to 5.3° larger than the low-speed cascade design angle of attack, and at element e, the difference is approximately 2.7° to 3.7°. It would seem, therefore, that the elements might well have been set at even larger angles of attack, especially at the hub section.

The low-loss angle-of-attack range at $1.00N_d$ is approximately 5° at all elements. At $0.81N_d$ the range would have been greater than 5°, but it was restricted on the low-angle-of-attack end by the test-facility flow resistance. The range at $1.11N_d$ is approximately 4° at all elements except element e where separation has increased losses at all angles of attack. The range at $1.21N_d$ is decreased to approximately 3°, and almost all of the decrease occurs at the lower angles of attack.

Efficiencies.- The peak blade-element-momentum efficiencies are 0.90 or more at all speeds and all blade elements except near the blade tip at $1.11N_d$ and $1.21N_d$. The only peak element efficiency at $1.11N_d$ which is less than 0.90 is at element e and is approximately 0.83. At the highest speed, $1.21N_d$, the peak η_M is less than 0.90 at elements d and e where the values are 0.87 and 0.69, respectively.

Turning angle θ_o.- The turning angles were obtained from the surveys made at approximately 1.5 inches upstream and downstream of the rotor in constant-area annuli in conjunction with rotational speeds. (See fig. 6(b), ref. 1.) It was assumed that the radial component of velocity was zero for each blade element. For the slope of the hub of this rotor, the influence of neglecting radial velocity should be only a few tenths of a degree in turning angle at the more inboard elements where the effect is greatest. The design turning angles are the turning angles required to fulfill the design vector diagrams and are indicated on the angle-of-attack—turning-angle curve of each element by a cross (+) mark (fig. 5).

The turning angle at element e is 1.5° less than the design value at $0.81N_d$ and $1.00N_d$. At the higher speeds of $1.11N_d$ and $1.21N_d$ the turning angle decreased quite rapidly because of flow separation in the tip region. Only the data for $1.21N_d$ showed a drop in turning angle at the next more inboard element d. The turning-angle data for other speeds at element d and all the speeds at elements b and c showed no apparent effect of Mach number for inlet relative Mach numbers up to 1.06. Elements b, c, and d produced turning angles which were from 1.0° to 1.6° larger than the design turning angle at the selected angle of attack.

At element a, the element nearest the hub, the curve of turning angle against angle of attack has a steeper slope than the curves at the other elements. This rapid decrease in turning angle at the lower angles of attack can be attributed to increased separation due to incipient choking. The decrease in relative inlet angle and increase in relative inlet Mach number which accompany the decrease in angle of attack are both effects which tend to worsen a choking-type condition. This increased separation at the lower angles of attack is probably the cause of the underturning of approximately 5° at the design point. There is no apparent explanation for the lower turnings (of the order of 3°) measured at $0.81N_d$.

Radial variation of $\frac{\Delta p}{(P - p)_{1R}}$ and D.- For all test speeds the diffusion factor D for all blade elements excluding the tipmost element e falls in a range between 0.26 and 0.58 which is below the limit value prescribed for low loss in reference 4. (Ref. 4 indicates that in order to achieve a low loss, 65-series and circular-arc blade sections should be operated at values of D below 0.45 in the tip region and less than 0.60 along the rest of the blade.)

At element e, (fig. 5(e)) the values of D are somewhat higher than at the more inboard elements and range from approximately 0.35 to 0.73. At the two higher speeds, where the values of D exceed the limiting value of 0.45, the losses are high and the efficiencies low. However, at $1.00N_d$ values of D as high as 0.54 were measured with an element

efficiency of 0.90 and a total-pressure-loss coefficient of 0.08. The minimum loss value of D at this speed is 0.43 with a corresponding efficiency of approximately 0.98.

The curves of static-pressure-rise coefficient against angle of attack are very similar in shape between all elements and speeds with values ranging from 0.20 to 0.50. The significance of the pressure-rise coefficient is in more detail in a subsequent paragraph.

In order to examine more closely the effect of blade loading as indicated by $\frac{\Delta p}{(P - p)_{1R}}$ and D on minimum total-pressure-loss coefficient $\bar{\omega}_{min}$, data from figure 5 have been replotted. The values of $\frac{\Delta p}{(P - p)_{1R}}$ and D used in this plot are those associated with minimum loss coefficient for each element at each speed. Figure 6(a) is a plot of minimum total-pressure-loss coefficient $\bar{\omega}_{min}$ against D. It can be seen that at a D value of approximately 0.53 the loss increased very rapidly at elements c and d while the more inboard elements did not reach the level of D where loss increased rapidly. At the outboard element e the rapid increase in loss occurred at a higher level of D; that is, something of the order of 0.58. At the blade tip, as separation occurs, there is a tendency for D to increase because of the influence of V_{a2}/V_{a1} which decreases markedly.

Figure 6(b) presents the variation of minimum total-pressure-loss coefficient $\bar{\omega}_{min}$ with static-pressure-rise coefficient. The more outboard three elements all reached a maximum value of $\frac{\Delta p}{(P - p)_{1R}}$ and then showed a decrease with increasing inlet Mach number. This maximum value of $\frac{\Delta p}{(P - p)_{1R}}$ was 0.43 at element e and increased to about 0.46 at element d. At elements b and c the maximum value was about 0.48, and at the most inboard element a the maximum value was 0.45. To summarize, excluding the tipmost element e, the range of maximum values of $\frac{\Delta p}{(P - p)_{1R}}$ was narrow (from 0.45 to 0.48). The corresponding inlet relative Mach numbers were as high as 1.03. Since for most transonic rotors it is the tip region which first exhibits flow separation, it appears that the determination of a tip-region loading limit is highly desirable. The flow in the tip region is complicated by tip-clearance effects, by centrifuged blade boundary layer piling up, and, for most transonic applications, by the highest inlet relative Mach numbers. Therefore, it is not surprising

to note that the tip-region loss increased at a lower $\frac{\Delta p}{(P - p)_{1R}}$ than did the other elements. The loss coefficient increased quite rapidly when $\frac{\Delta p}{(P - p)_{1R}}$ reached 0.43 and the inlet relative Mach number was approximately 1.01.

It is believed that working levels of $\frac{\Delta p}{(P - p)_{1R}}$ can be established by comparing the limiting values for this rotor with that of other transonic rotors. A working level thus established would be applicable to other rotors similar to those used to establish the value. Then any rotor which either failed to reach this level or greatly exceeded it could be studied in detail to determine the reasons for the performance obtained.

Comparison of tip $\frac{\Delta p}{(P - p)_{1R}}$ and D for several transonic rotors.- Several other transonic rotors have been examined to determine their tip region limiting $\frac{\Delta p}{(P - p)_{1R}}$ values. The results are presented in figure 7(a) which is a plot of the minimum total-pressure-loss coefficients at several rotational speeds against $\frac{\Delta p}{(P - p)_{1R}}$. The data from references 6 and 7 represent a blade element located 12.7 percent of the blade height from the tip and from reference 5, a blade element located 16.5 percent of the blade height from the tip. The data given from the subject rotor represent an element 10.8 percent of the blade height from the tip. The relative inlet Mach numbers associated with the data for the rotors from references 5, 6, and 7 are approximately 1.1 for the highest $\bar{\omega}_{min}$ of each rotor. The double-circular-arc blading tested at the three solidities of 0.66, 0.88, and 1.04 (refs. 6 and 7) showed a systematic increase in the maximum value of $\frac{\Delta p}{(P - p)_{1R}}$ with solidity, although the values for the solidities of 0.88 and 1.04 differed very little (from 0.37 to 0.40). No large increase in maximum value of $\frac{\Delta p}{(P - p)_{1R}}$ was noted for the data for $\sigma = 1.32$ (ref. 5); however, only two speeds were presented for this rotor, and test results for some lower speeds might indicate a higher limiting value of $\frac{\Delta p}{(P - p)_{1R}}$. The results for the rotor presented in the current report ($\sigma = 0.78$) indicated a somewhat higher limiting value of $\frac{\Delta p}{(P - p)_{1R}}$ (0.43) than that of the

double-circular-arc blade of comparable solidity. Hence, the results presented in figure 7(a) indicate that near the tip for σ values from 0.78 to 1.32 and relative inlet Mach numbers near 1.0, the range of limiting $\frac{\Delta p}{(P - p)_{1R}}$ values is from 0.37 to 0.43. The data for σ of 0.66 did show high loss at a lower $\frac{\Delta p}{(P - p)_{1R}}$ level of 0.315. Therefore, it appears to be desirable to avoid solidities below 0.75 in the tip region. Also, these results indicate that for Mach numbers near 1.1 values of $\frac{\Delta p}{(P - p)_{1R}}$ greater than 0.37 to 0.43 invariably produced flow separation for the rotors examined.

The values of D associated with the data of figure 7(a) are presented in figure 7(b). The band of data obtained from a large number of conventional rotors and stators in reference 4 is indicated on this plot by dashed lines. Almost all the test points fall within this band; however, the curves show a rapid increase in minimum loss at widely different values of D.

The establishment of a limit parameter capable of properly accounting for the flow phenomena in a compressor would require: (1) a detailed analysis of extensive blade-element pressure-distribution data for wide ranges of transonic cascade conditions, and (2) a method of estimating the surface pressure distributions at transonic speeds. Since these data are not available and accurate methods of estimating surface pressure distributions for conditions at transonic speeds are not available, the alternative in attempting to establish a design loading-limit rule is to use gross-limit parameters which can be determined without knowledge of the blade-element pressure distributions. The inadequacy of such parameters will be reflected by different limit levels as they fail to effectively account for the flow taking place in the blading.

Presentation of Radial Variation of Several Blade-Element Parameters

The radial variations in M_{1R}, M_2, $\left(g\rho_2 V_{a2}\right)_F$, P_2/P_1, p_2/p_1, and η_M for all test points presented in this paper are presented in figures 8 to 13. Many of these data were previously discussed in the blade-element section. The data are presented in more detailed form here to facilitate the use of the results for additional analysis. Each figure represents one of the preceding parameters and has four plots which present the four speeds, $0.81N_d$, $1.00N_d$, $1.11N_d$, and $1.21N_d$. In order to

make the plots more readable, the vertical scale is shifted upward one grid unit for each successive throttle position. The complete scale is for the lowest curve, which represents the open-throttle or high-flow condition. Each succeeding curve represents a lower weight flow condition with the top curve representing the near-surge condition. It might be pointed out that the $(g\rho_2 V_{a2})_F$ values plotted in figure 10 are measured values for test conditions having upstream stagnation pressures of approximately 20 inches of mercury.

Comparison Between Design and Measured Rotor Performance

In order to evaluate the degree of design control that existed for this rotor, a comparison between design and measured rotor performance was made. The original rotor design was computed for air (ref. 8, appendix A); however, as stated previously, the test data were obtained in a Freon atmosphere. Since the pressure ratios are different for the same turning angle in Freon and in air (ref. 1), it was necessary to calculate the Freon design values that correspond to the original air design values. This calculation was done by assuming that Freon and air design inlet Mach numbers, relative inlet air angles, turning angles and efficiencies were the same and by satisfying simple radial equilibrium $\left(\frac{dp}{dr} = \rho \frac{V_\theta^2}{r}\right)$ and continuity. The design values shown as dashed lines in figures 14(a) to 14(h) were obtained from this computation. The test data presented in these plots are for three weight flows at design speed: (1) the maximum weight flow of 54.6 lb/sec, which is very near design weight flow of 55.0 lb/sec, (2) the peak efficiency weight flow of 51.8 lb/sec, and (3) the near-surge weight flow of 47.9 lb/sec. The effects of nonconstant inlet static pressure and inlet swirl on entering conditions may be observed by comparing the inlet conditions determined from test results at 54.6 lb/sec with the design values (figs. 14(a) and 14(b)). Mach numbers were only slightly lower than the design values. Relative inlet angles agreed quite well with design from the hub to the mean but decreased from the mean to the tip, where the measured angle was approximately 2.0° below the design value.

Turning angle θ_o.- A comparison between measured and design turning angles θ_o is presented in figure 14(c). In the middle portion of the annulus, the agreement was good (within 0.9°). The turning angles near the tip and hub were considerably below the design values. It should be pointed out, however, that at design flow (55.0 lb/sec) efficiency decreased quite rapidly in the tip region (fig. 14(d)); hence, the lower turning angles in the tip region were caused, in part, by flow separation as well as the lower-than-design inlet angle indicated in figure 14(b).

Outlet flow angle, β_2.- The outlet flow angles β_2 on stationary coordinates are presented in figure 14(e). The measured angles at the near-design flow of 54.6 lb/sec are several degrees less than the design values except near the tip. This result is a consequence of the weight flow distribution $g\rho_2 V_{a2}$ which is presented in figure 14(f). The tip-region flow separation has resulted in a greater level of $g\rho_2 V_{a2}$ for the more inboard portion of the rotor. The $(g\rho_2 V_{a2})_F$ values plotted in figure 14(f) are corrected to standard conditions of pressure and temperature. This inward shift of weight flow is also noticeable in the plot of V_{a2}/V_{a1}, figure 14(g).

Total pressure ratio P_2/P_1.- The variation in total pressure ratio P_2/P_1 is presented in figure 14(h). The lower-than-design turning angles in the hub and tip regions in conjunction with the lower tip-region efficiencies (fig. 14(d)) and the higher axial-velocity ratios at the hub account for the lower-than-design total pressure ratio at the hub and tip for the near-design weight flow of 54.6 lb/sec. At the two lower weight flows, the pressure ratios do not decrease as rapidly near the tip as in the high-flow case.

$\frac{\Delta p}{(P - p)_{1R}}$ and D.- A comparison between design and measured values of loading parameters D and $\frac{\Delta p}{(P - p)_{1R}}$ is presented in figure 14(i). The measured data represent only the near-design weight flow of 54.6 lb/sec. The values of D are less than design all along the blade height, with the maximum difference occurring near the hub. The $\frac{\Delta p}{(P - p)_{1R}}$ values agree fairly well with design; however, the slope of the test values is different from design, with lower-than-design values in the hub region and higher-than-design values in the tip region. This departure from the design values is partially caused by the axial velocity ratios which are higher than design at the hub and lower than design at the tip.

Design control conclusions.- The prime purpose of presenting this comparison is to point out to what extent it is possible to predict the performance of a rotor designed for an exploratory study at rather extreme conditions when using available design data. It appears that although the low-speed cascade data were quite effective in estimating turning angles over much of the blade, design control as far as β_2, V_{a2}/V_{a1}, P_2/P_1, D, and $\frac{\Delta p}{(P - p)_{1R}}$ prediction could be improved. While part of

this lack of accurate control resulted from tip-region separation, it is obvious that good design should endeavor to avoid separation. Since this transonic rotor was designed for operation at considerably higher specific weight flows than previous rotors, as well as a lower solidity level, it is not surprising to find the design control to be somewhat deficient in several respects. The comparison indicates the need for more exact methods of estimating efficiencies, turning angles near the blade ends, and the radial distribution of exit flow at these Mach numbers and total-pressure ratios.

SUMMARY OF RESULTS

A detailed examination of blade-element performance at five radial locations ranging from 8.3 percent of the blade height away from the inner casing to 10.8 percent away from the outer casing indicated the following:

1. At the design rotor speeds of 0.81, 1.00, and 1.11 minimum-loss coefficients were low for all the blade elements with the exception of the most outboard element at 1.11 design rotor speed. The maximum relative inlet Mach number associated with these low-loss coefficients was 1.04.

2. The minimum-loss angle of attack occurred at an angle approximately 3° to 4° larger than the selected angle near the hub and approximately 0° to 1° larger than the selected angle near the tip. Since the selected angles of attack were larger than the low-speed cascade design angles of attack, it appeared that the minimum loss occurred approximately 4.3° to 5.3° above low-speed cascade design near the hub and 2.7° to 3.7° above near the tip.

3. The low-loss angle-of-attack range was approximately 5° at all elements at design speed and approximately 4° at all elements except near the tip at 11 percent above design speed.

4. At 21 percent above design speed severe separation occurred in the tip region at all angles of attack tested with the Mach numbers ranging from 1.08 to 1.22.

5. For all elements exclusive of the tipmost element, the range of maximum values of the static-pressure-rise coefficient for which minimum losses were low was quite narrow and ranged from 0.45 to 0.48. The corresponding inlet relative Mach numbers were as high as 1.03.

6. In the tip region minimum-loss coefficients increased quite rapidly when the static-pressure-rise coefficient reached 0.43 and the relative inlet Mach number was above approximately 1.01.

7. The low-speed cascade data were fairly effective for the estimation of design turning angles at relative inlet Mach numbers as high as 1.06 for the main portion of the annulus which was free of flow separation and three-dimensional flow effects.

8. A comparison between design and measured flow conditions indicated that better design control is desirable. In order to improve design control at these Mach numbers and pressure ratio levels, it will be necessary to accurately estimate the radial variation in blade element efficiency, flow distribution, and turning angles near the blade ends.

An examination of several other transonic rotors in the tip region indicated the following:

1. For solidity values of from 0.78 to 1.32 and relative inlet Mach numbers near 1.0, the range of limiting static-pressure-rise coefficient values at which loss coefficient increased rapidly was from 0.37 to 0.43.

2. At a solidity of 0.66 the maximum value of the static-pressure-rise coefficient at which losses increased rapidly was 0.315. Hence, it appears desirable to avoid solidities much less than 0.75.

3. The limiting diffusion factor values showed a rather wide variation for the several rotors.

Langley Aeronautical Laboratory,
National Advisory Committee for Aeronautics,
Langley Field, Va., November 8, 1956.

APPENDIX

SHADOWGRAPHS OF ROTOR IN OPERATION

Shadowgraph photographs of the rotor used were taken through a window in the outer casing in the plane of the rotor. The shadowgraphs were taken at three speeds of $1.00N_d$, $1.11N_d$, and $1.21N_d$ throughout the range of throttle settings. The test setup and procedure are described in detail in reference 9. The shadowgraphs were taken both as random still pictures and as motion-picture sequences.

Figure 15 is a typical shadowgraph photograph taken in this test program. In order to clarify interpretation of this photograph, labels have been attached to the significant parts. The distinct shadow of the tip section of the blade is clearly seen on the rotor hub which was painted white for this reason. Also, the shock wave at the leading edge of the blade may be readily identified. The rotor blade itself appears fuzzy and out of focus because the camera was focused on the hub. The relative positions of the rotor blade and its shadow on the hub place the light source on the upper right of the picture as well as out from the page. The front and rear edges of the rotor hub are also easily identified.

Six more typical shadowgraphs at maximum flow are presented for three speeds of $1.00N_d$ (fig. 16(a)), $1.11N_d$ (fig. 16(b)), and $1.21N_d$ (fig. 16(c)). The two pictures in each of the three parts of this figure show the same shock system and differ in only the position of the rotor blade. It becomes apparent from an examination of these photographs that because the area of the hub is small for this 0.35 hub-tip ratio rotor, it is possible to capture only a portion of the shock system existing at a given rotor running condition (i.e., speed and flow rate) in a single photograph. Therefore, in order to obtain a complete picture of the shock system it is necessary to take many photographs with the blade "stopped" in different positions. Because these shadowgraphs are presented as samples and show only a portion of the shock waves, discussion of the shock systems is not given until the discussion of figure 17. However, it should be pointed out that the dark lines across the passage in the plane of rotation in both pictures of part (a) for $1.00N_d$ are oil and are not to be confused with shock waves. It is felt that a casing-boundary-layer separation may cause the oil to form this definite line in the plane of rotation.

A large number of shadowgraphs were taken, and in order to summarize them, three composite sketches were made. (See fig. 17.) The

blade sections and the geometry shown in these sketches represent the tip blade element since almost all the shock waves seen in these shadowgraphs are at this radial location. Parts (a), (b), and (c) of figure 17 show the speeds of $1.00N_d$, $1.11N_d$, and $1.21N_d$, respectively. The position of the shock wave at open throttle or maximum flow condition is indicated by a solid line. At the near-stall condition, the shock wave is marked by a dashed line. The line marking the end of all of the shock waves upstream of the blades is the extent of the photograph and not necessarily the end of the shock wave.

At $1.00N_d$ for the open throttle condition (fig. 17(a)) the shock wave passes ahead of the leading edge of one blade and stands on the suction surface of the next blade at approximately the 0.85 chord point. The relative inlet Mach number at this condition at the blade tip is 1.06 and the section efficiency is 0.67. As the back pressure is increased by throttling, the shock wave moves forward until, at the near-stall condition it is standing on the suction surface of the blade at approximately the 0.45 chord position. The efficiency has increased to 0.79 and the relative inlet Mach number has decreased to 0.99. (The efficiencies and Mach numbers mentioned herein were measured at the outermost blade element, element 1, of fig. 4.)

For the maximum flow condition at $1.11N_d$ (fig. 17(b)) the bow shock wave becomes oblique and for all practical purposes attaches to the leading edge of the blade. The shock extends across the passage and ends on the separated flow slightly downstream of the trailing edge of the blade. An oblique shock emanates from the point of separation (about the 0.85-chord point) and intersects the normal shock. Also an area of supersonic flow exists on the pressure surface of the blade at the leading edge between the oblique shock and the normal shock. The tip section efficiency has dropped to 0.45 and the inlet relative Mach number is 1.17. At the near-stall condition the shock has moved out of the passage and stands on the suction surface at the 0.55-chord location. The section efficiency is 0.76 and the inlet relative Mach number is 1.12.

The general arrangement of the shock system at the open throttle condition of the highest speed tested, $1.21N_d$ (fig. 17(c)) is similiar to that of $1.11N_d$ (fig. 17(b)). A normal shock spans the passage and stands on the blade-pressure surface on one side and on the separated flow slightly downstream of the trailing edge on the other side. The angle of the oblique shock attached to the leading edge is decreased due to the higher inlet relative Mach number of 1.27, and the region of supersonic flow on the pressure surface is also larger. The section efficiency for this condition is 0.35. When the back pressure is increased by throttling, the shock moves forward out of the passage and stands at the 0.76-chord point on the suction surface. The inlet relative Mach number at this condition is 1.21 and the section efficiency is 0.65.

REFERENCES

1. Savage, Melvyn, and Felix, A. Richard: Investigation of a High-Performance Axial-Flow Compressor Transonic Inlet Rotor Designed for 37.5 Pounds Per Second Per Square Foot of Frontal Area - Aerodynamic Design and Overall Performance. NACA RM L55A05, 1955.

2. Dunavant, James C., Emery, James C., Walch, Howard C., and Westphal, William R.: High-Speed Cascade Tests of the NACA 65-$(12A_{10})10$ and NACA 65-$(12A_2I_{8b})10$ Compressor Blade Sections. NACA RM L55I08, 1955.

3. Felix, A. Richard: Summary of 65-Series Compressor-Blade Low-Speed Cascade Data by Use of the Carpet-Plotting Technique. NACA RM L54H18a, 1954.

4. Lieblein, Seymour, Schwenk, Francis C., and Broderick, Robert L.: Diffusion Factor for Estimating Losses and Limiting Blade Loadings in Axial-Flow-Compressor Blade Elements. NACA RM E53D01, 1953.

5. Sandercock, Donald M., Lieblein, Seymour, and Schwenk, Francis C.: Experimental Investigation of an Axial-Flow Compressor Inlet Stage Operating at Transonic Relative Inlet Mach Numbers. IV - Stage and Blade-Row Performance of Stage With Axial-Discharge Stators. NACA RM E54C26, 1954.

6. Lewis, George W., Jr., and Schwenk, Francis C.: Experimental Investigation of a Transonic Axial-Flow-Compressor Rotor With Double-Circular-Arc Airfoil Blade Sections. II - Blade-Element Performance. NACA RM E54J08, 1955.

7. Schwenk, Francis C., and Lewis, George W., Jr.: Experimental Investigation of a Transonic Axial-Flow-Compressor Rotor With Double-Circular-Arc Airfoil Blade Sections. III - Comparison of Blade-Element Performance With Three Levels of Solidity. NACA RM E55F01, 1955.

8. Savage, Melvyn, and Beatty, Loren A.: A Technique Applicable to the Aerodynamic Design of Inducer-Type Multistage Axial-Flow Compressors. NACA TN 2598, 1952.

9. Goldberg, Theodore J., and Sterrett, James R.: Use of Shadowgraph Technique in the Analysis of the Performance of Two Supersonic Axial-Flow Compressor Rotors Operating Over a Mean Radius Relative Inlet Mach Number Range of 0.85 to 1.7. NACA RM L56A05, 1956.

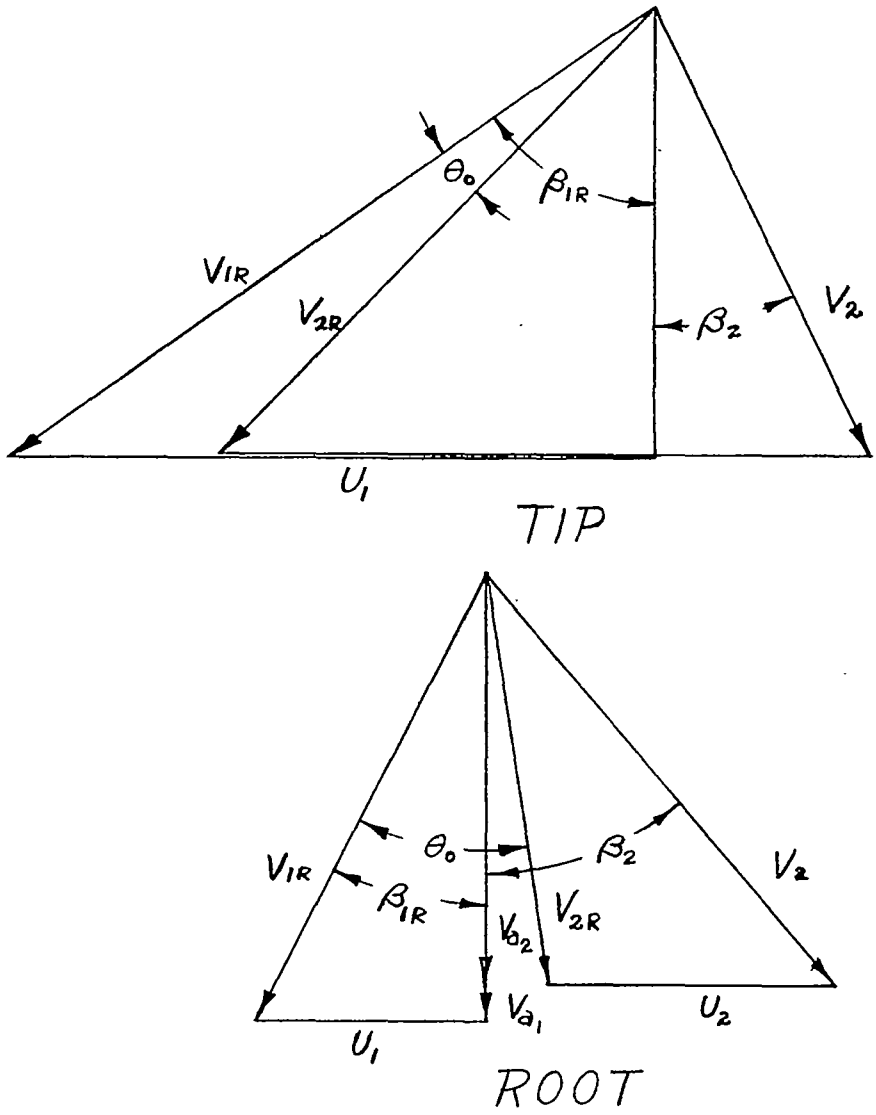

VELOCITY-DIAGRAM DATA

r_1/r_t	r_2/r_t	P_2/P_1	M_{1R}	β_{1R}	θ_o	D	$\frac{\Delta p}{(P - p)_{1R}}$	V_{a_2}/V_{a_1}	β_2	M_2
0.350	0.450	1.250	0.70	26.7	34.7	0.41	0.30	0.92	40.3	0.74
.585	.646	1.275	.82	40.1	20.3	.47	.41	.92	33.1	.66
.750	.787	1.300	.93	47.2	14.2	.44	.38	.94	29.3	.65
.883	.902	1.325	1.02	51.8	11.9	.41	.34	.96	27.0	.65
1.000	1.000	1.350	1.10	55.2	11.1	.39	.32	.99	25.6	.66

Figure 1.- Velocity-diagram design data in air (ref. 1).

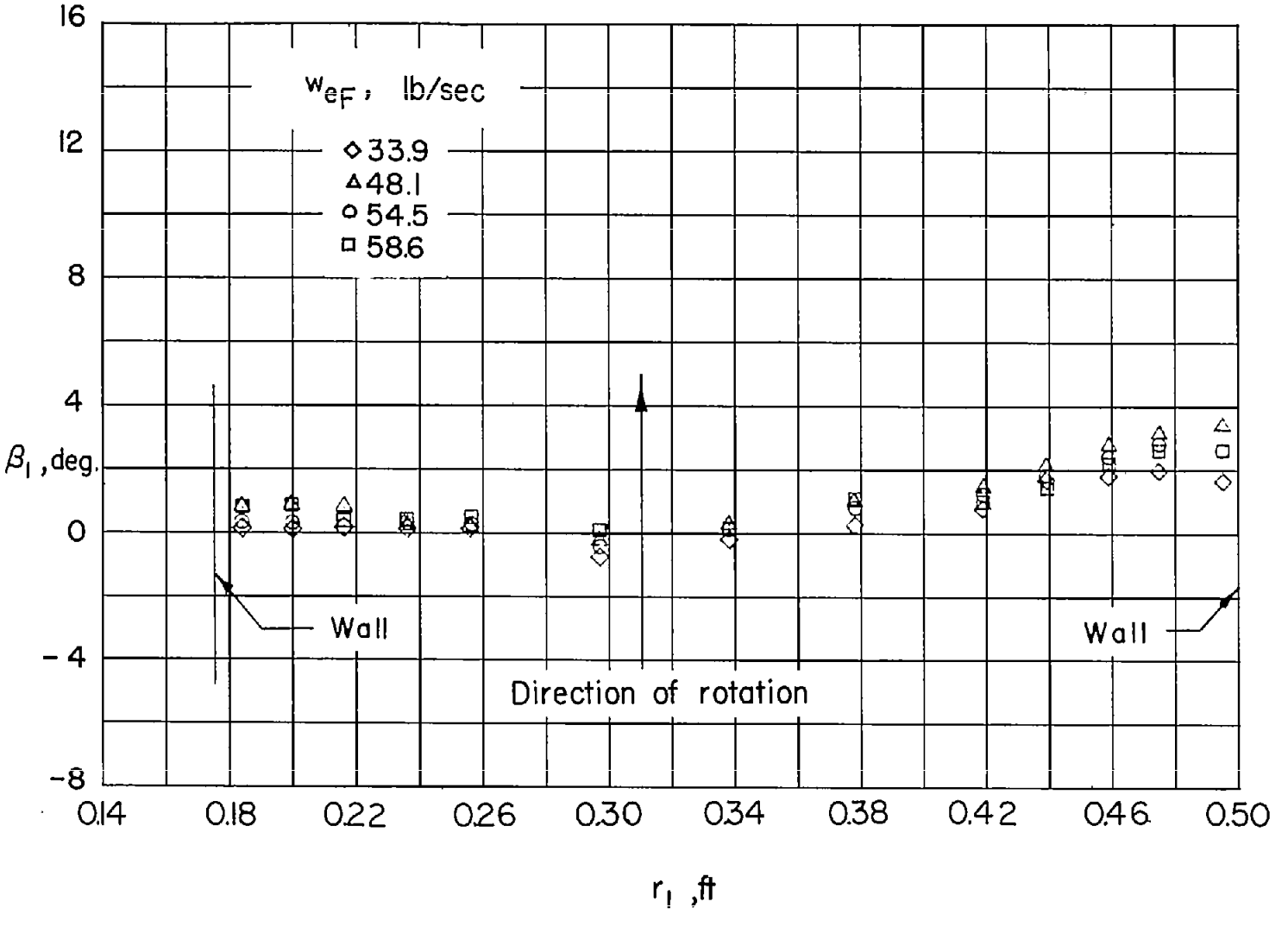

Figure 2.- Radial distribution of swirl ahead of the rotor at four weight flows.

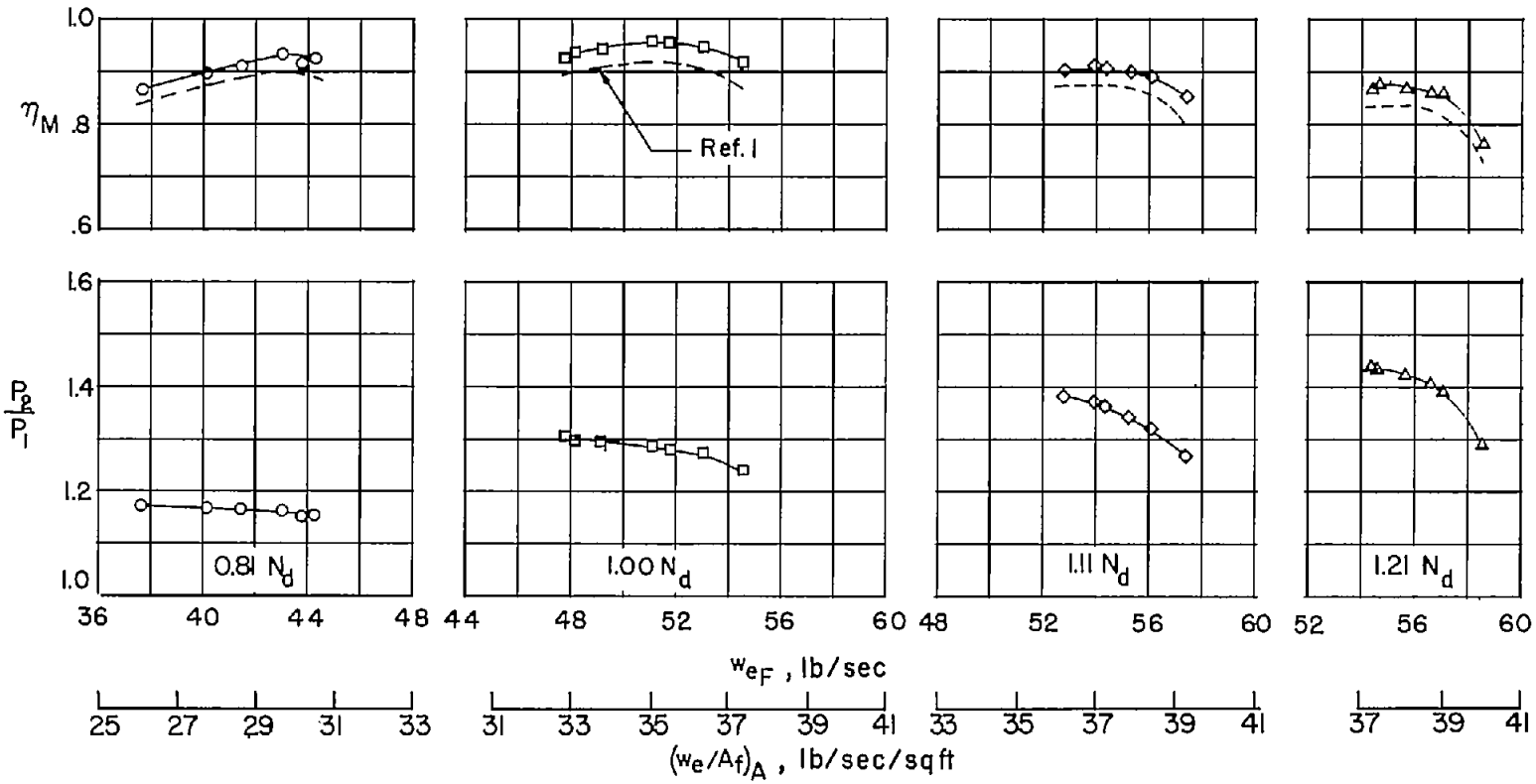

Figure 3.- Overall performance characteristics.

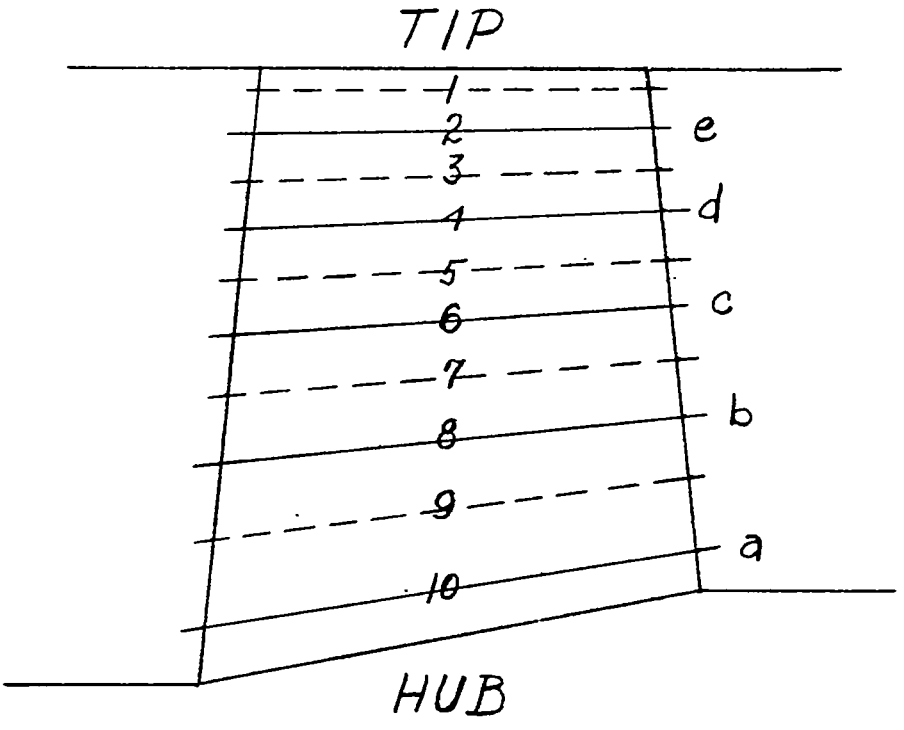

Equal-area centers			Element designation	Percent blade height (average) from outer casing
	r_1, ft	r_2, ft		
1	0.489	0.490		
2	.466	.469	e	10.8
3	.442	.447		
4	.416	.425	d	26.5
5	.389	.400		
6	.360	.375	c	44.2
7	.328	.347		
8	.292	.317	b	65.2
9	.252	.284		
10	.204	.246	a	91.7

Figure 4.- Equal-area centers.

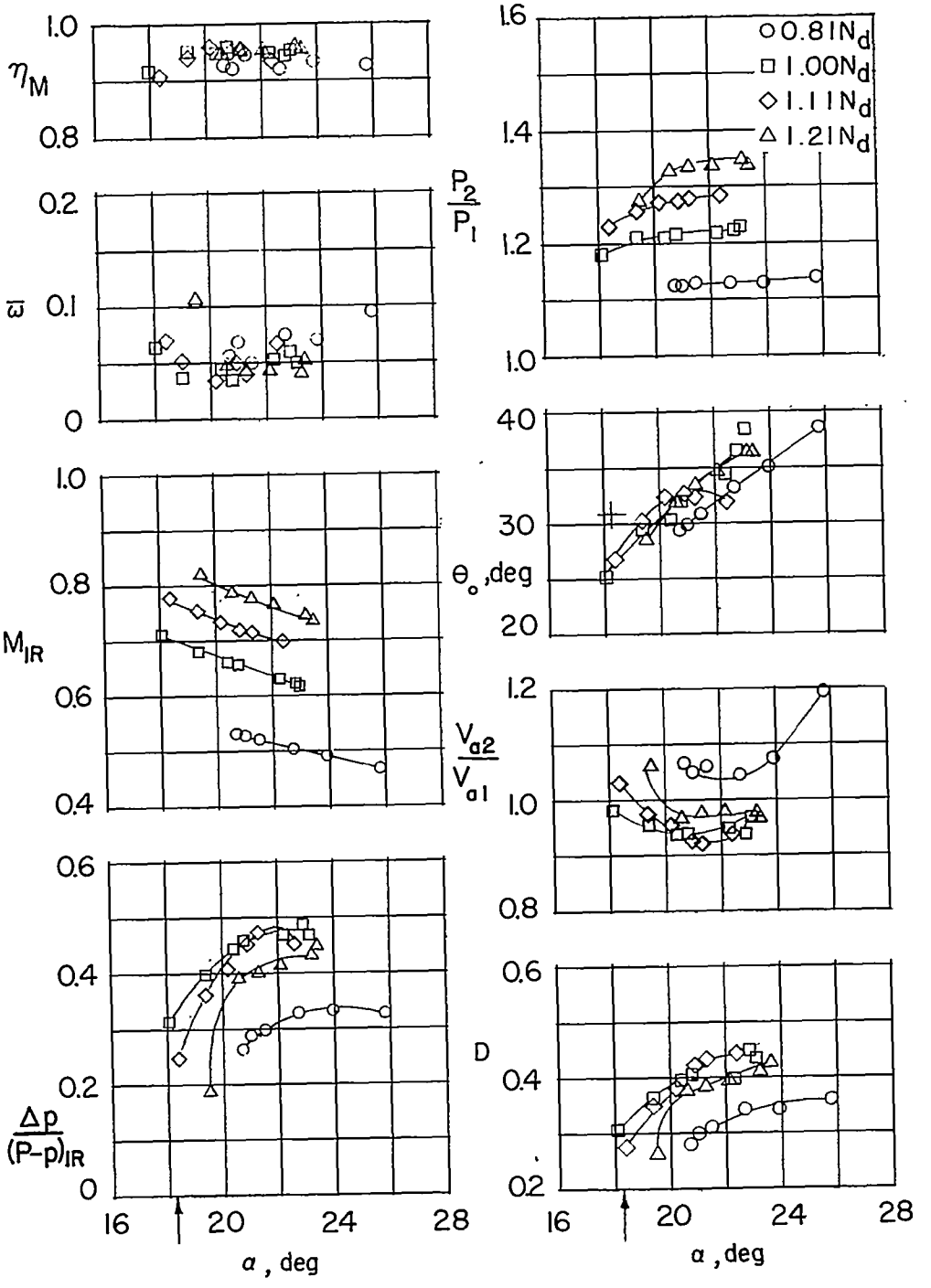

(a) r_1 = 0.204 foot; $\Delta\alpha'$ = 1.3°.

Figure 5.- Blade-element characteristics.

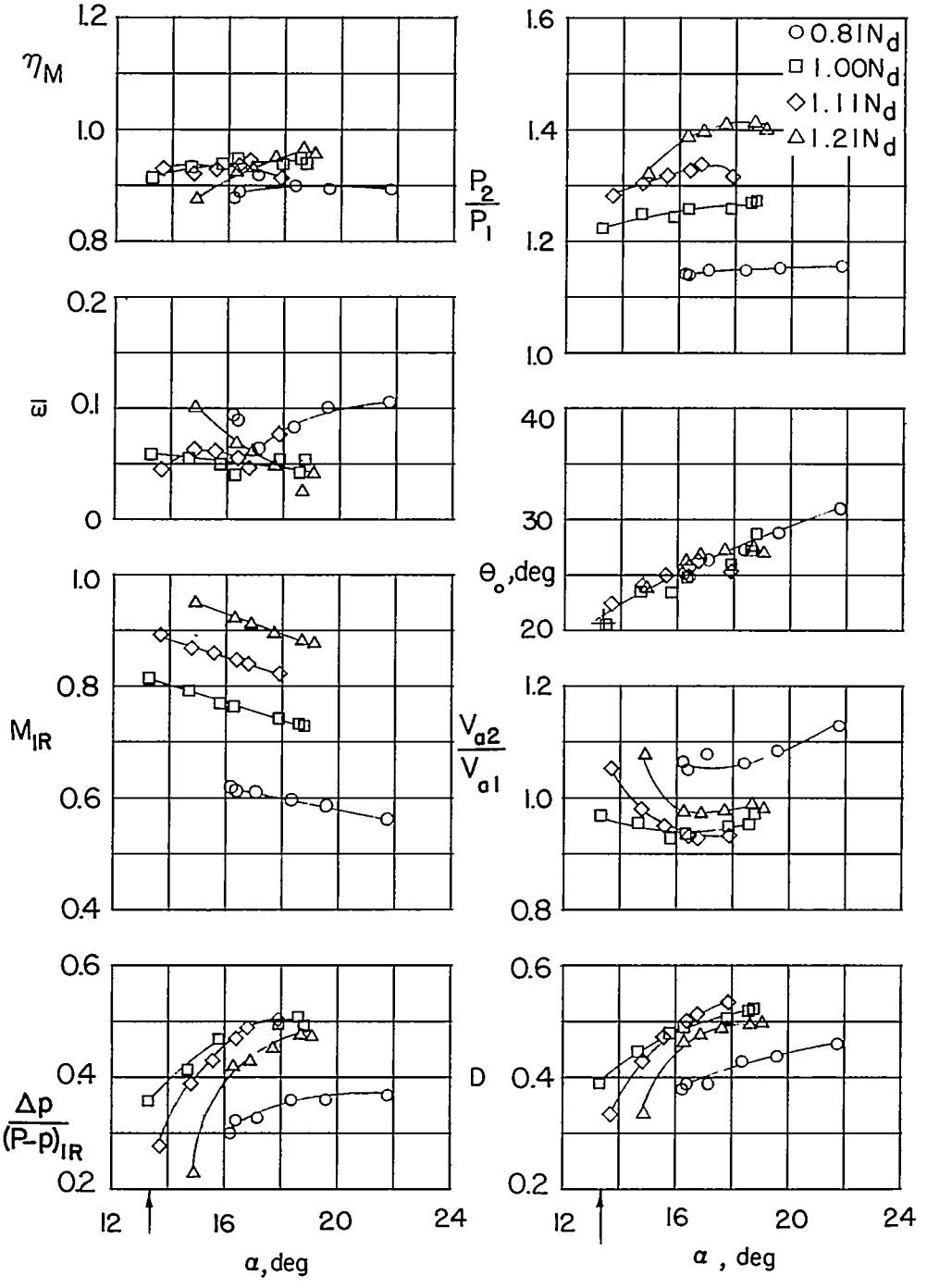

(b) r_1 = 0.292 foot; $\Delta\alpha'$ = 1.4°.

Figure 5.- Continued.

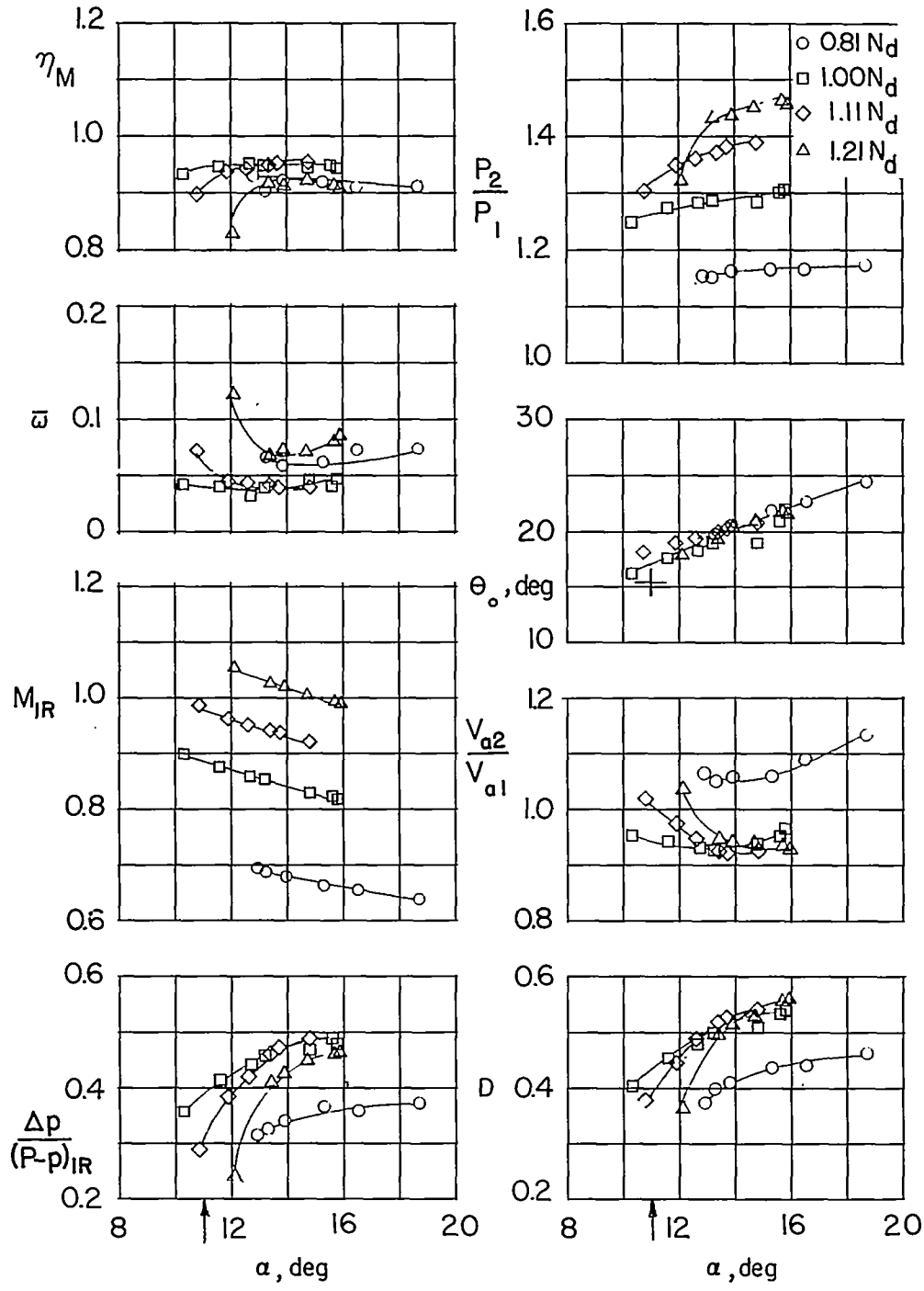

(c) r_1 = 0.360 foot; $\Delta\alpha'$ = 1.8°.

Figure 5.- Continued.

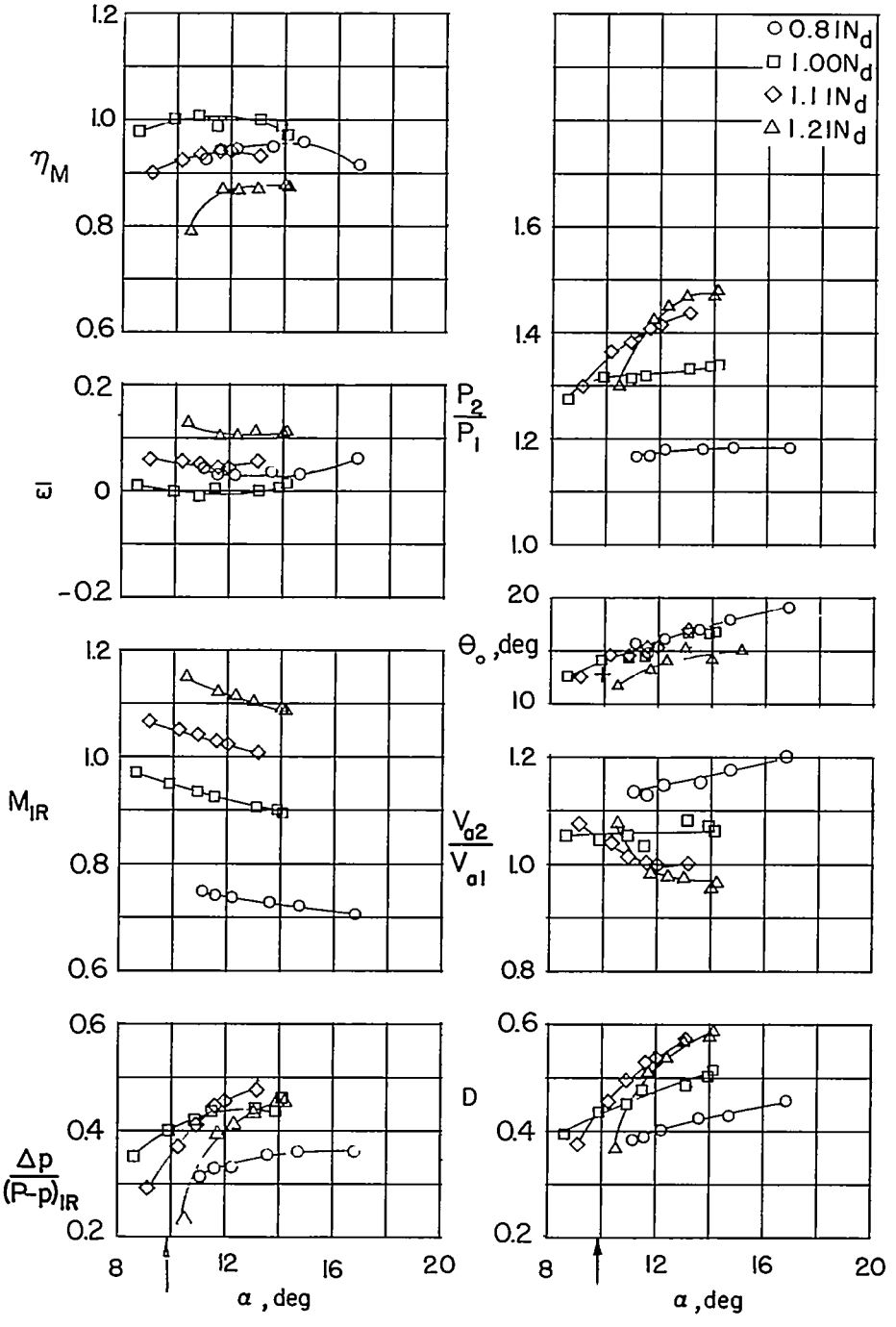

(d) r_1 = 0.416 foot; $\Delta\alpha'$ = 2.3°.

Figure 5.- Continued.

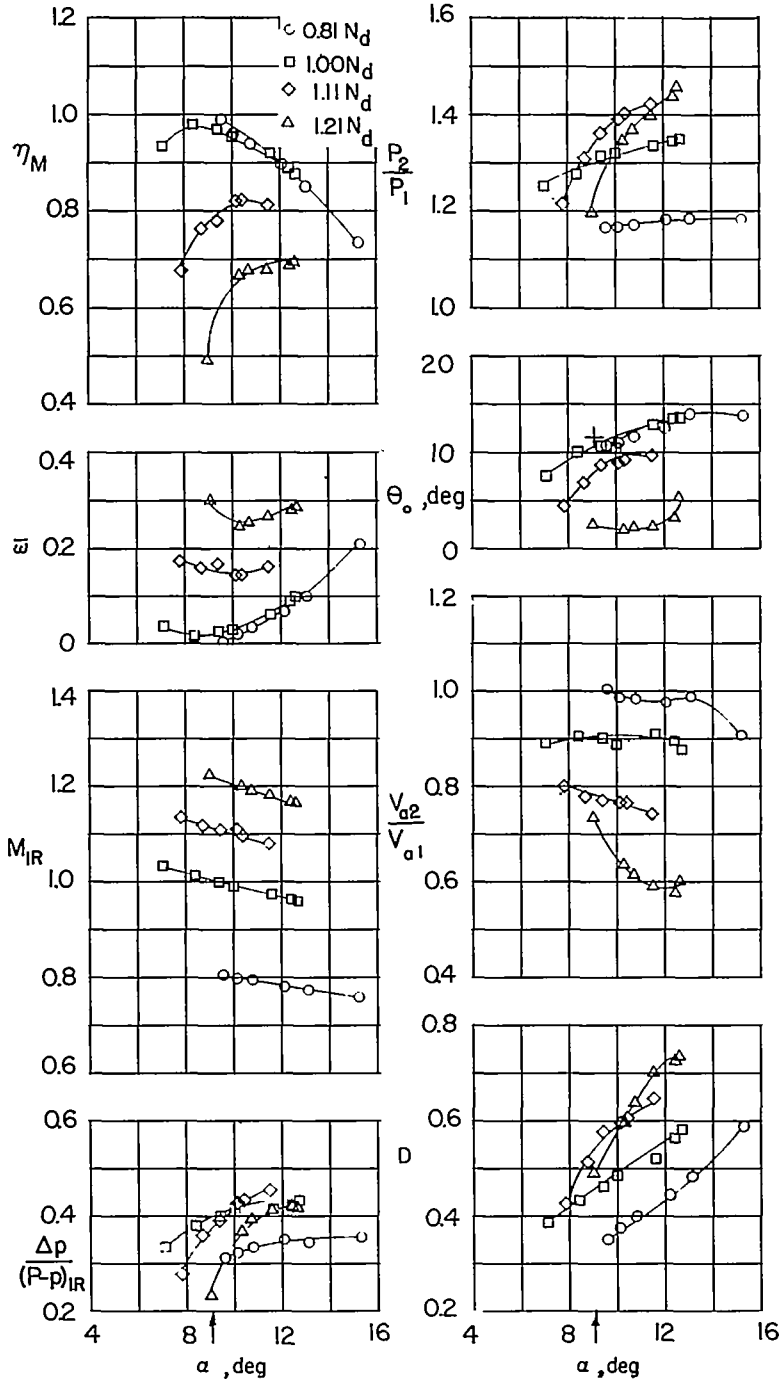

(e) r_1 = 0.466 foot; $\Delta\alpha'$ = 2.7°.

Figure 5.- Concluded.

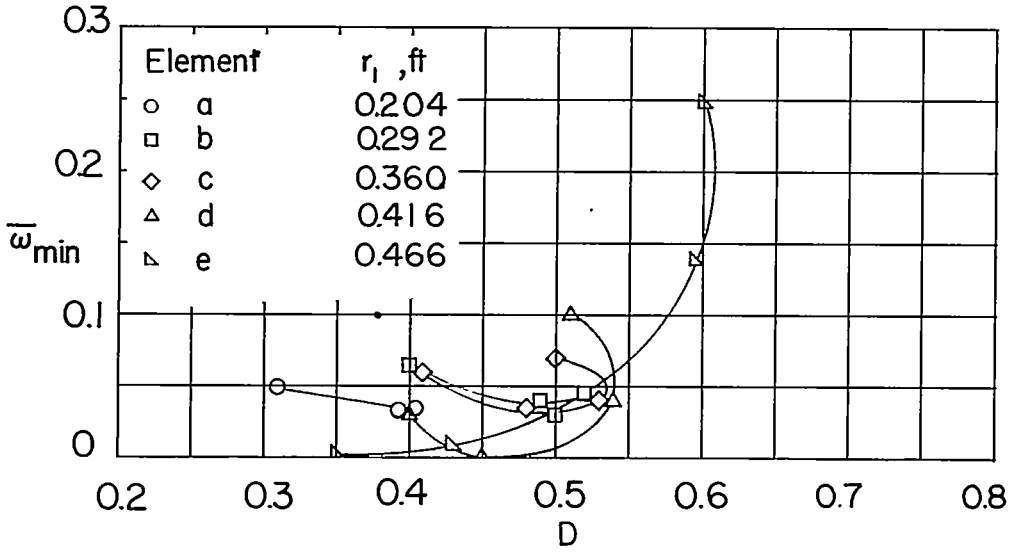

(a) Diffusion factor D.

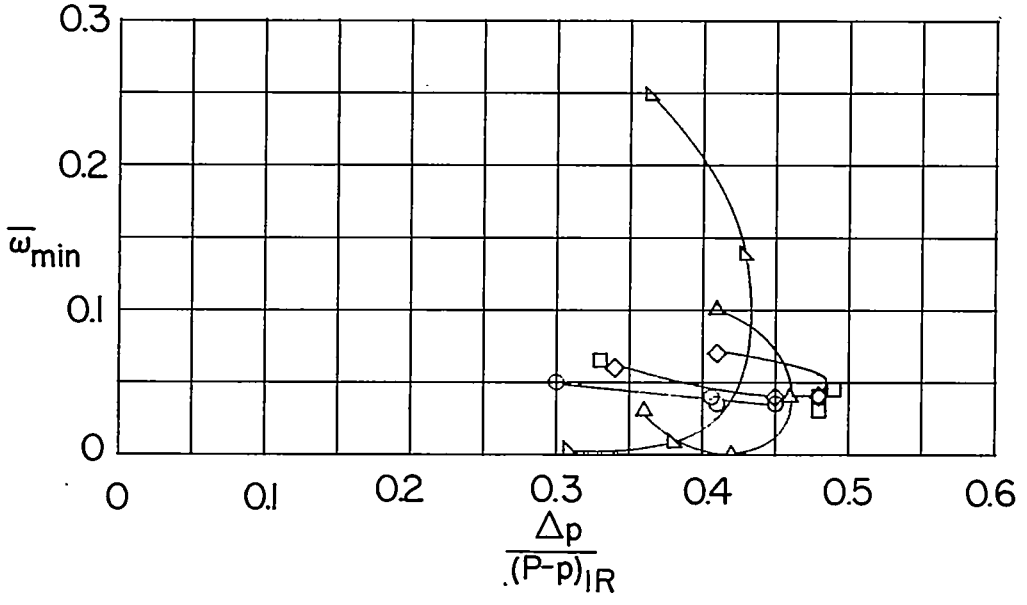

(b) Static-pressure-rise coefficient $\frac{\Delta p}{(P - p)_{1R}}$.

Figure 6.- Variation of minimum total pressure loss with $\frac{\Delta p}{(P - p)_{1R}}$ and D factor for five blade elements.

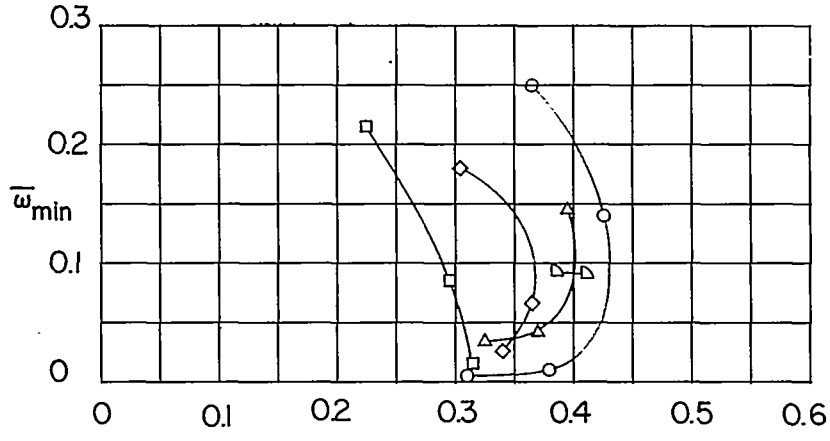

(a) Static-pressure-rise coefficient $\frac{\Delta p}{(P - p)_{1R}}$.

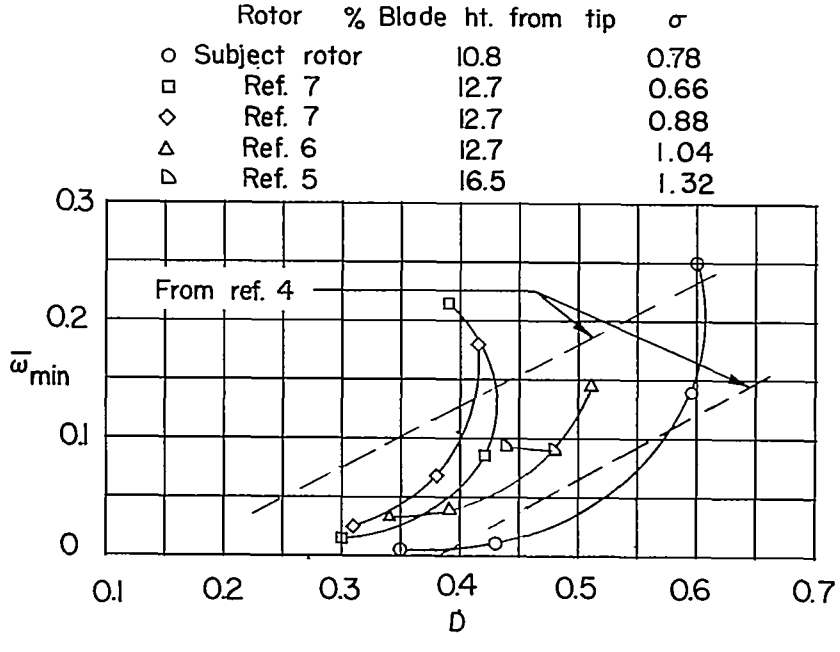

(b) Diffusion factor D.

Figure 7.- Variation of minimum total pressure loss with $\frac{\Delta p}{(P - p)_{1R}}$ and D factor near the tip of five transonic rotors including the present rotor.

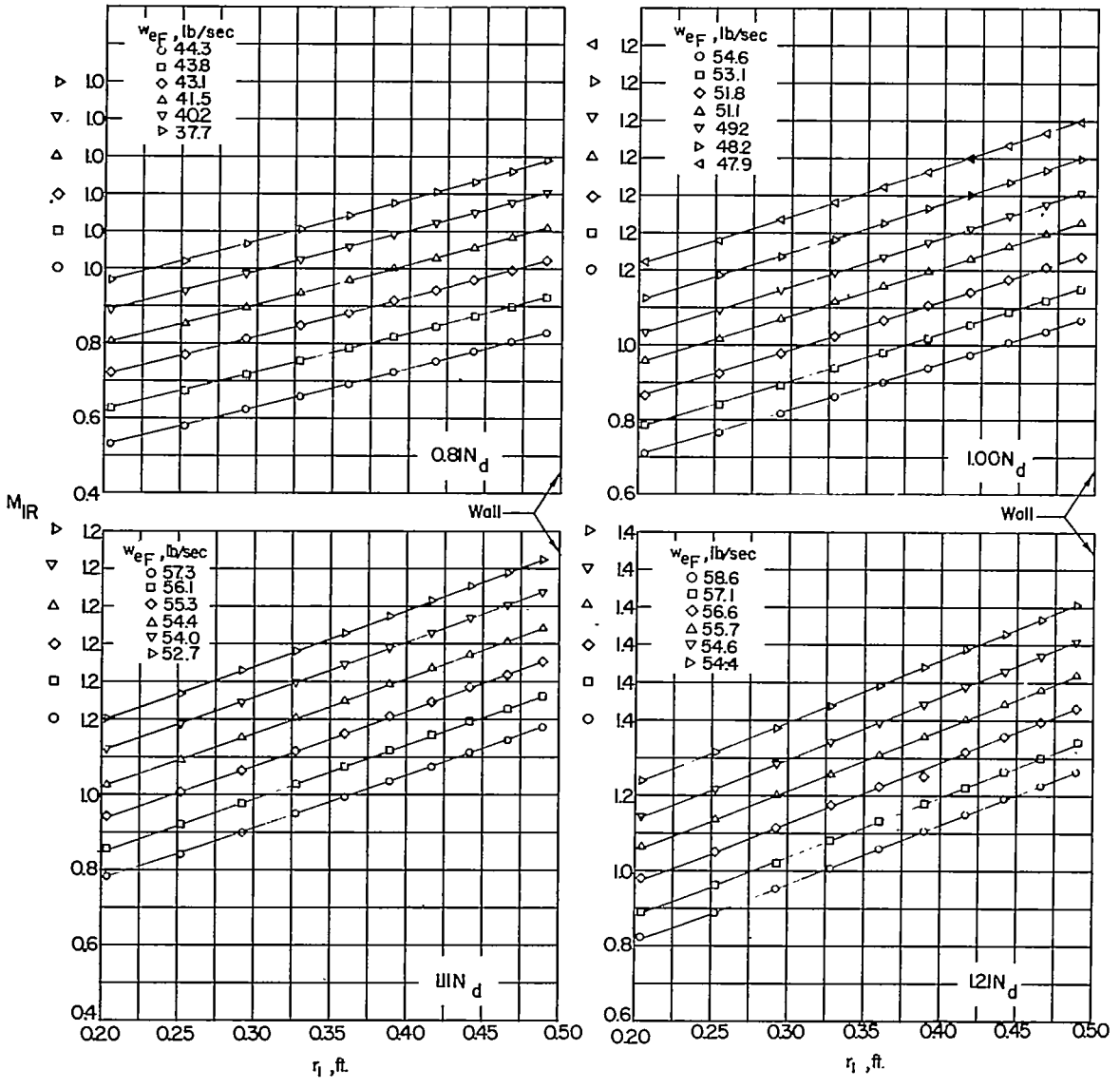

Figure 8.- Radial variation of relative inlet Mach number. The radius of the inner wall is 0.175 foot.

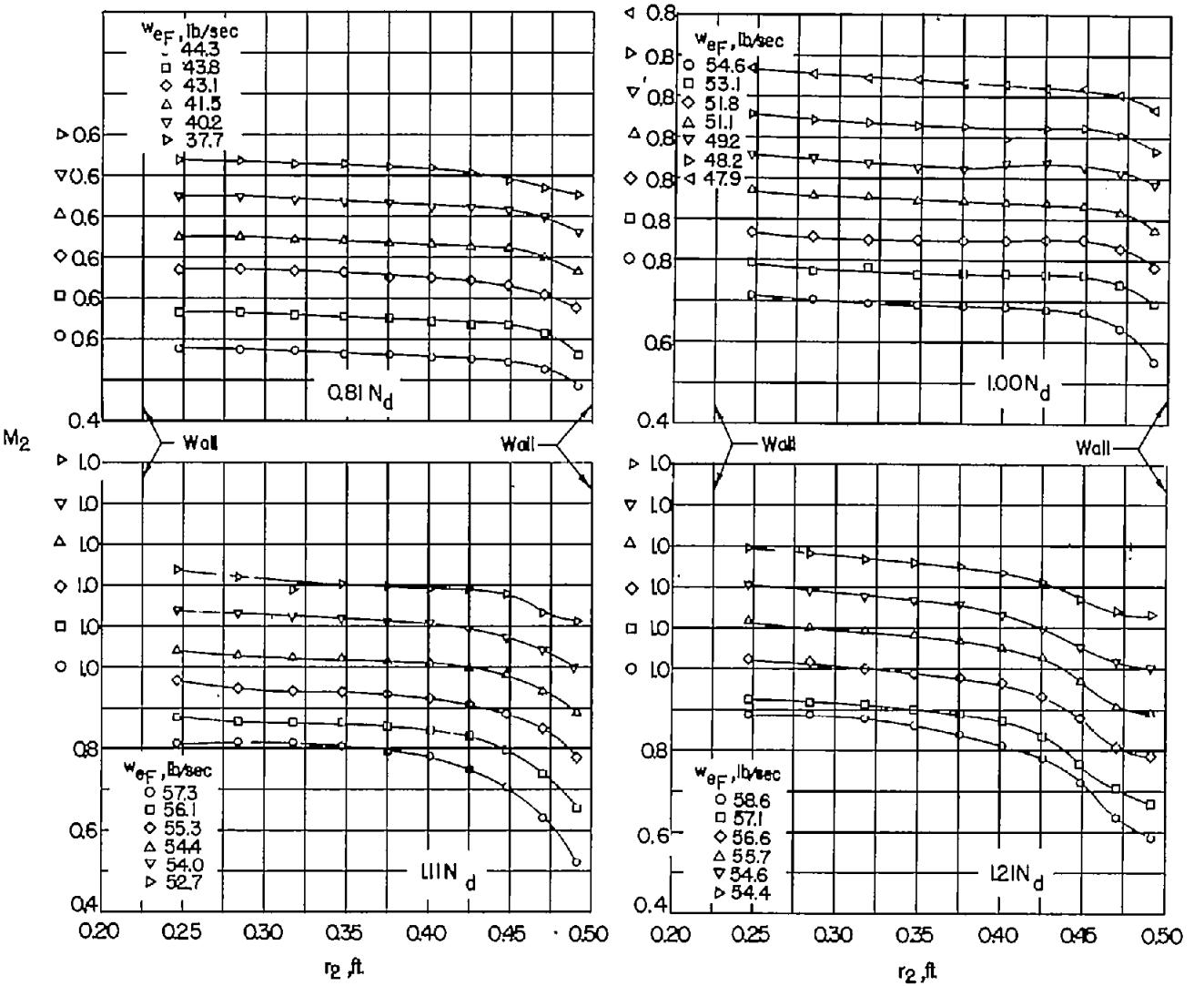

Figure 9.- Radial variation of absolute outlet Mach number.

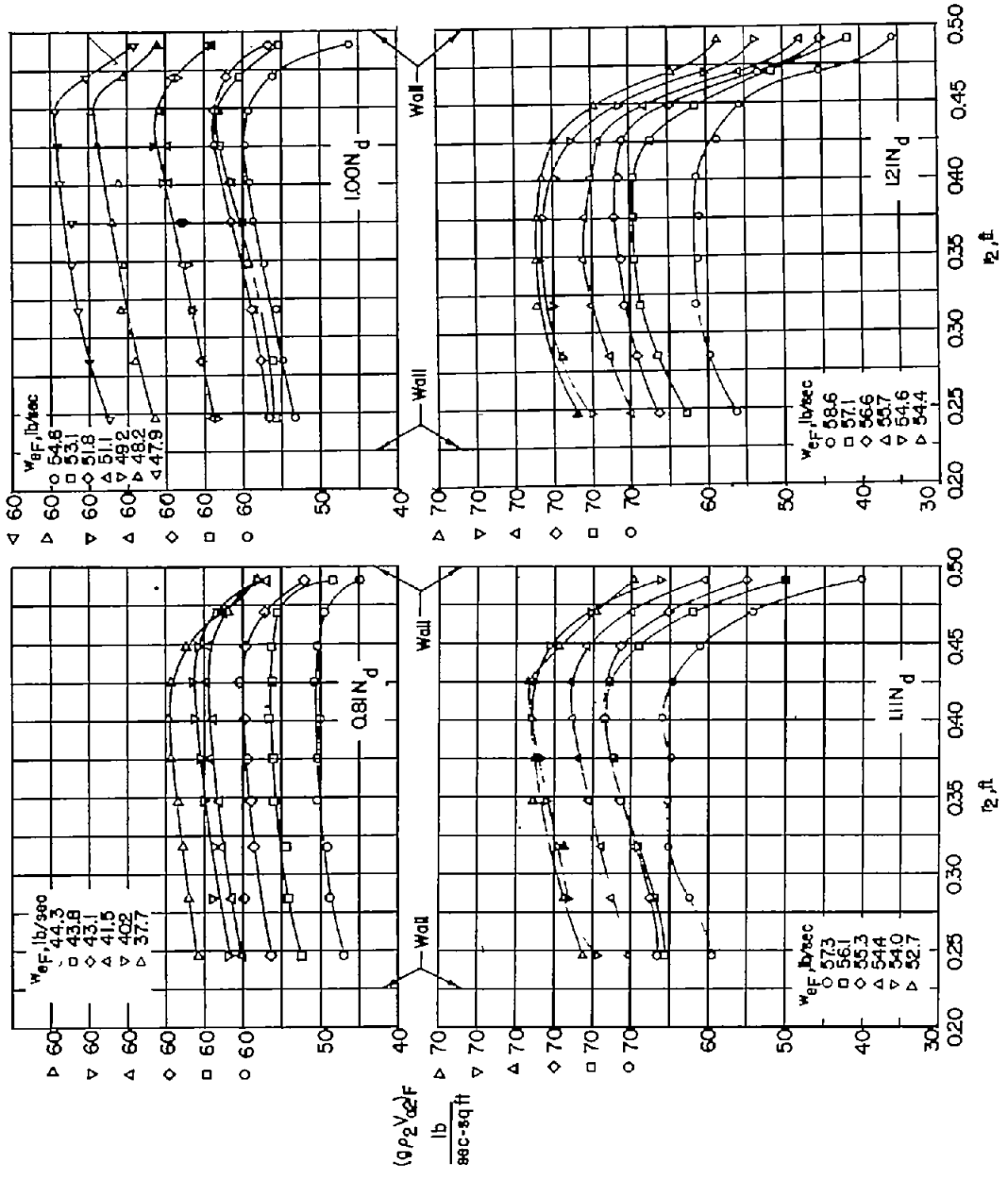

Figure 10.- Radial variation of outlet weight flow.

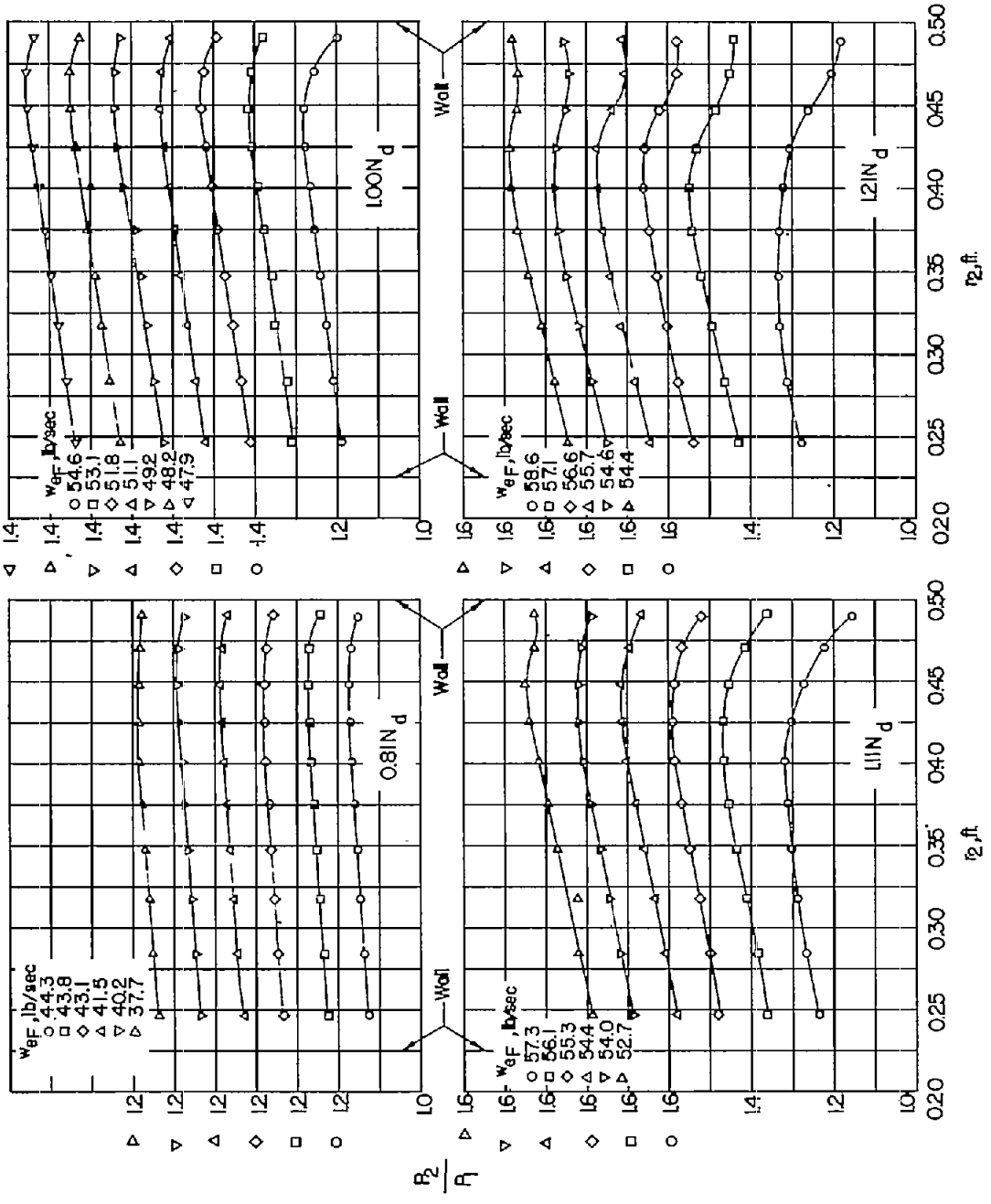

Figure 11.- Radial variation of total pressure ratio.

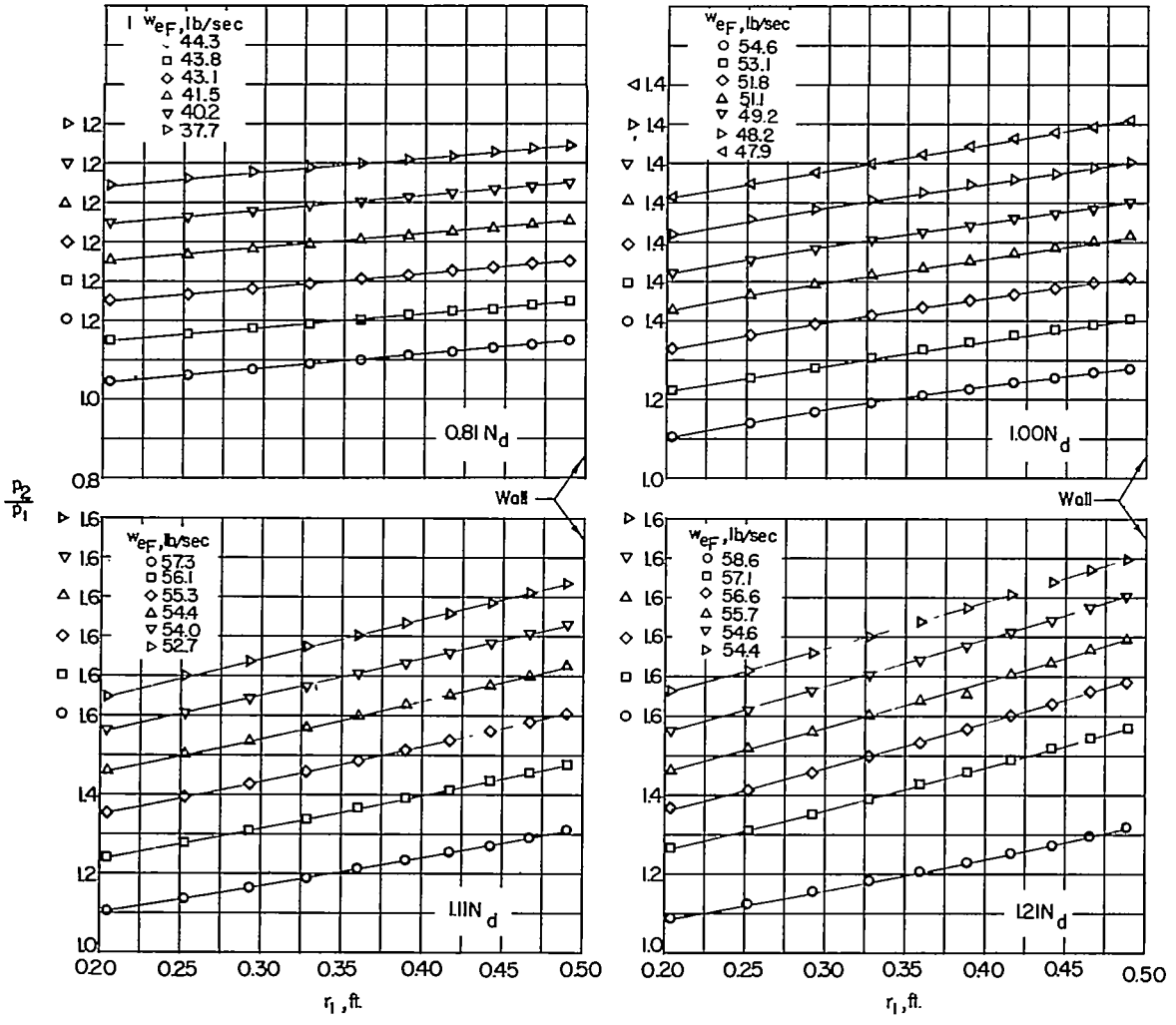

Figure 12.- Radial variation of static pressure ratio. The radius of the inner wall is 0.175 foot.

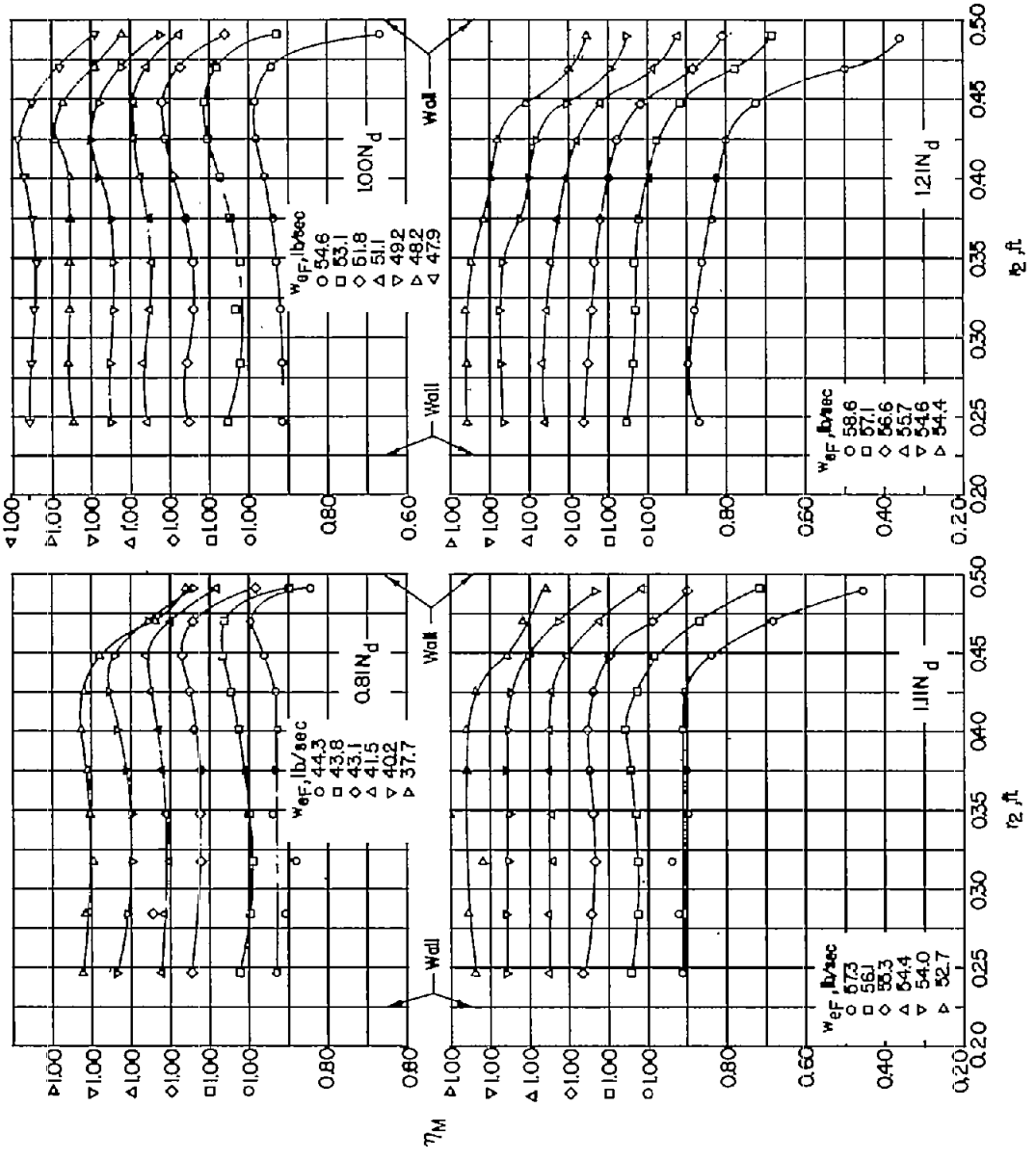

Figure 13.- Radial variation of momentum efficiency.

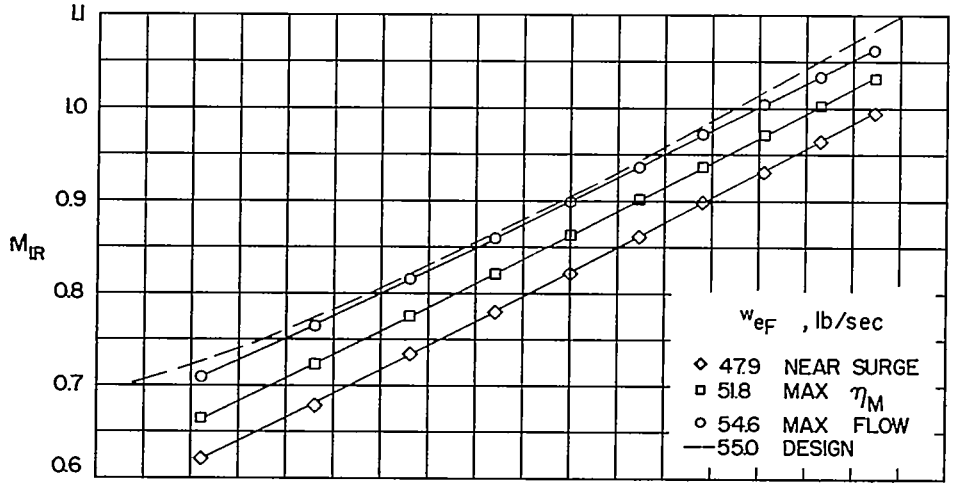

(a) Relative inlet Mach number M_{1R}.

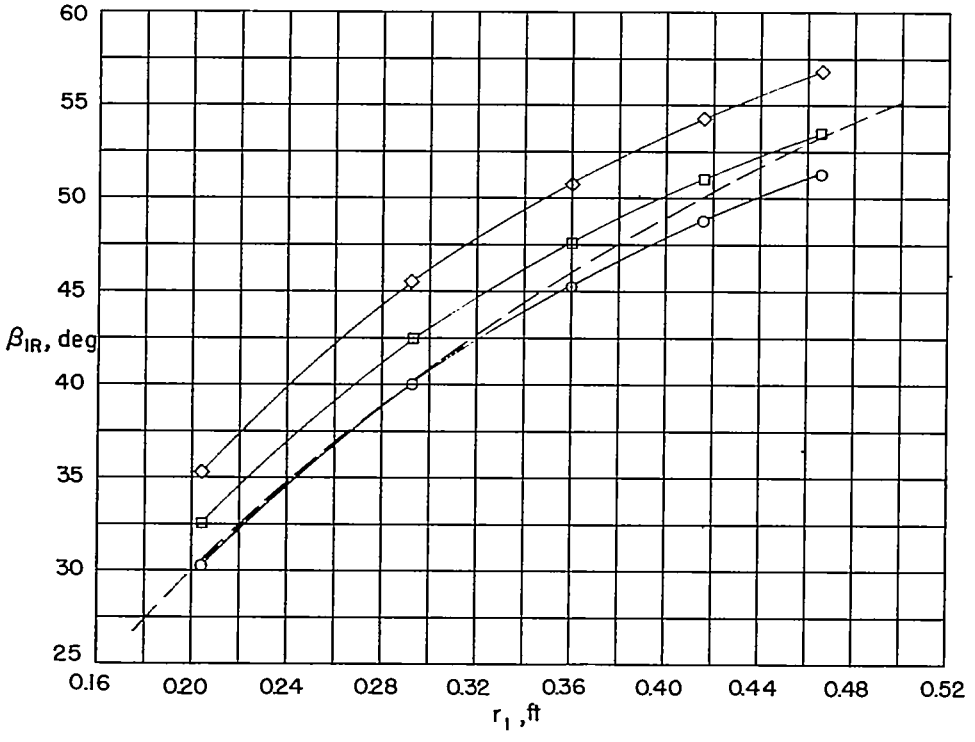

(b) Relative inlet flow angle β_{1R}.

Figure 14.- Comparison of design and measured flow parameters at design speed.

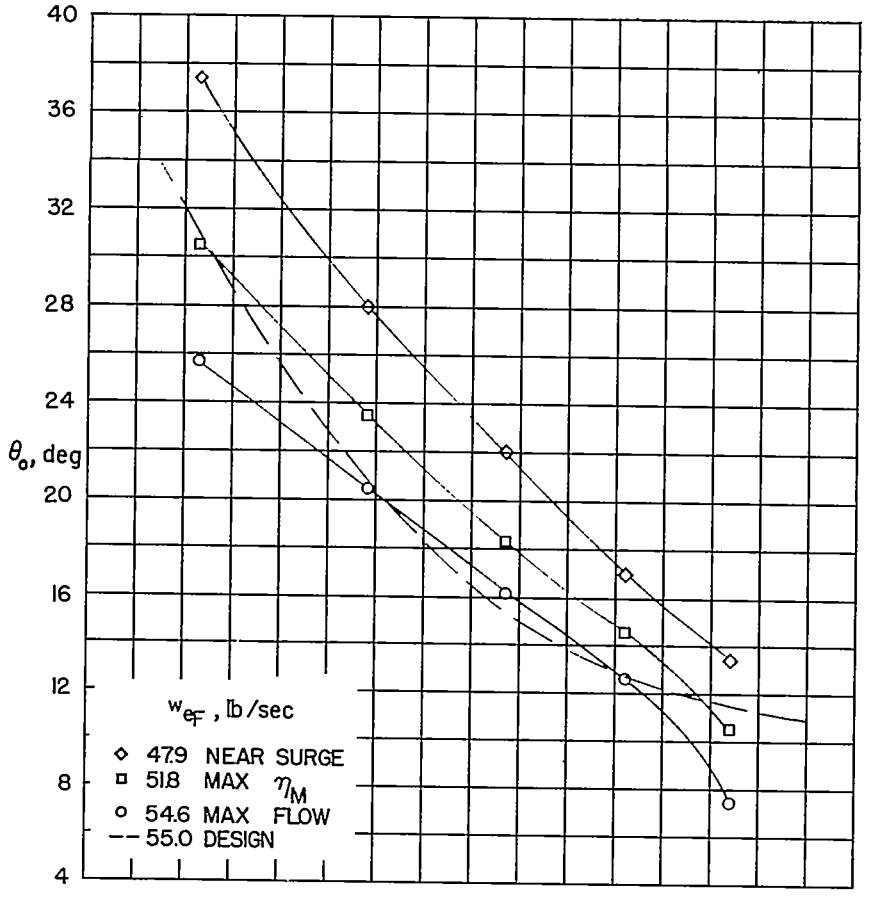

(c) Turning angle θ_o.

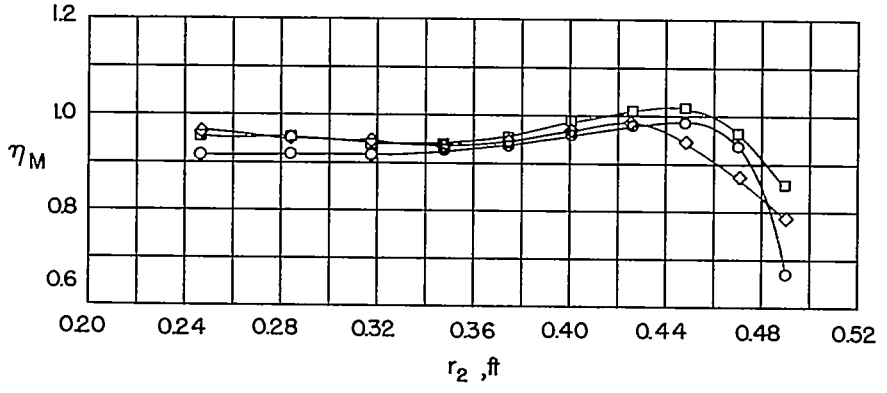

(d) Momentum efficiency η_M.

Figure 14.- Continued.

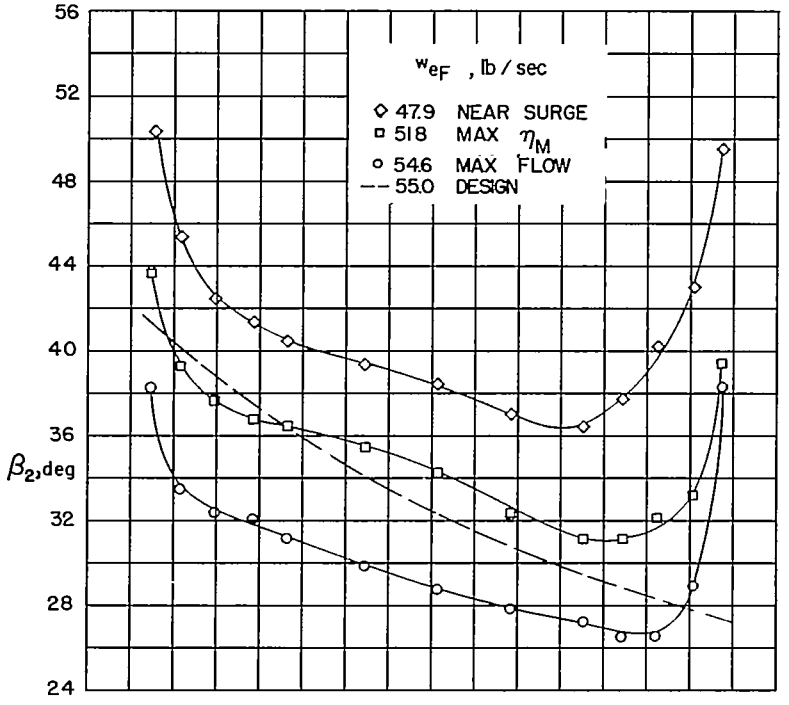

(e) Outlet flow angle β_2.

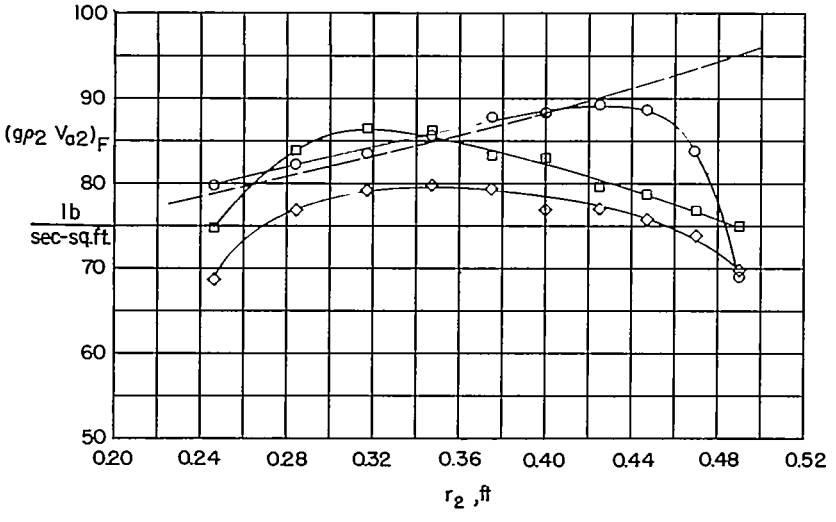

(f) Outlet weight flow $\rho_2 V_{a2}$.

Figure 14.- Continued.

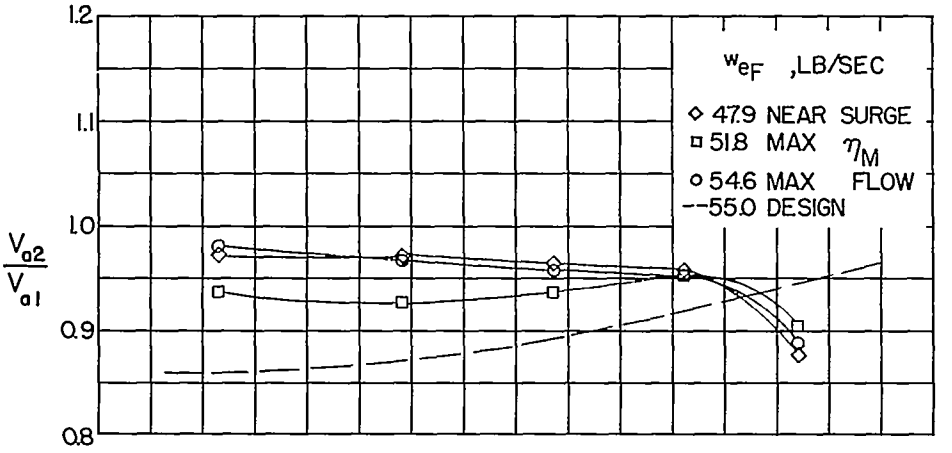

(g) Axial velocity ratio V_{a2}/V_{a1}.

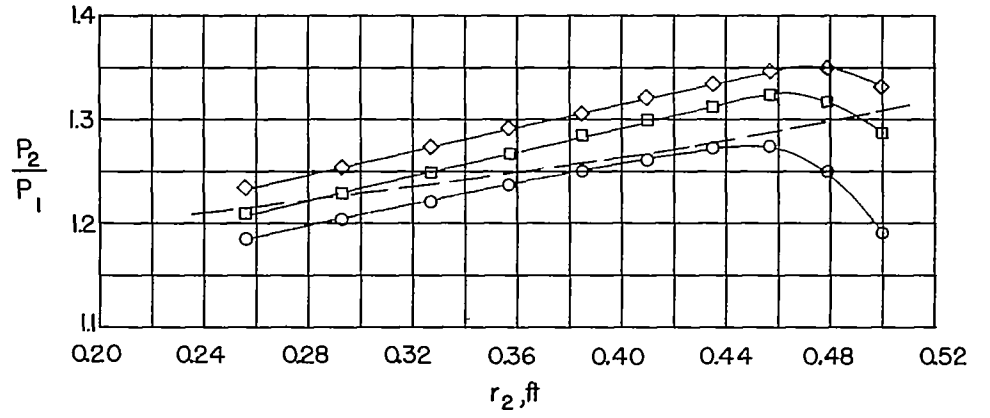

(h) Total pressure ratio P_2/P_1.

Figure 14.- Continued.

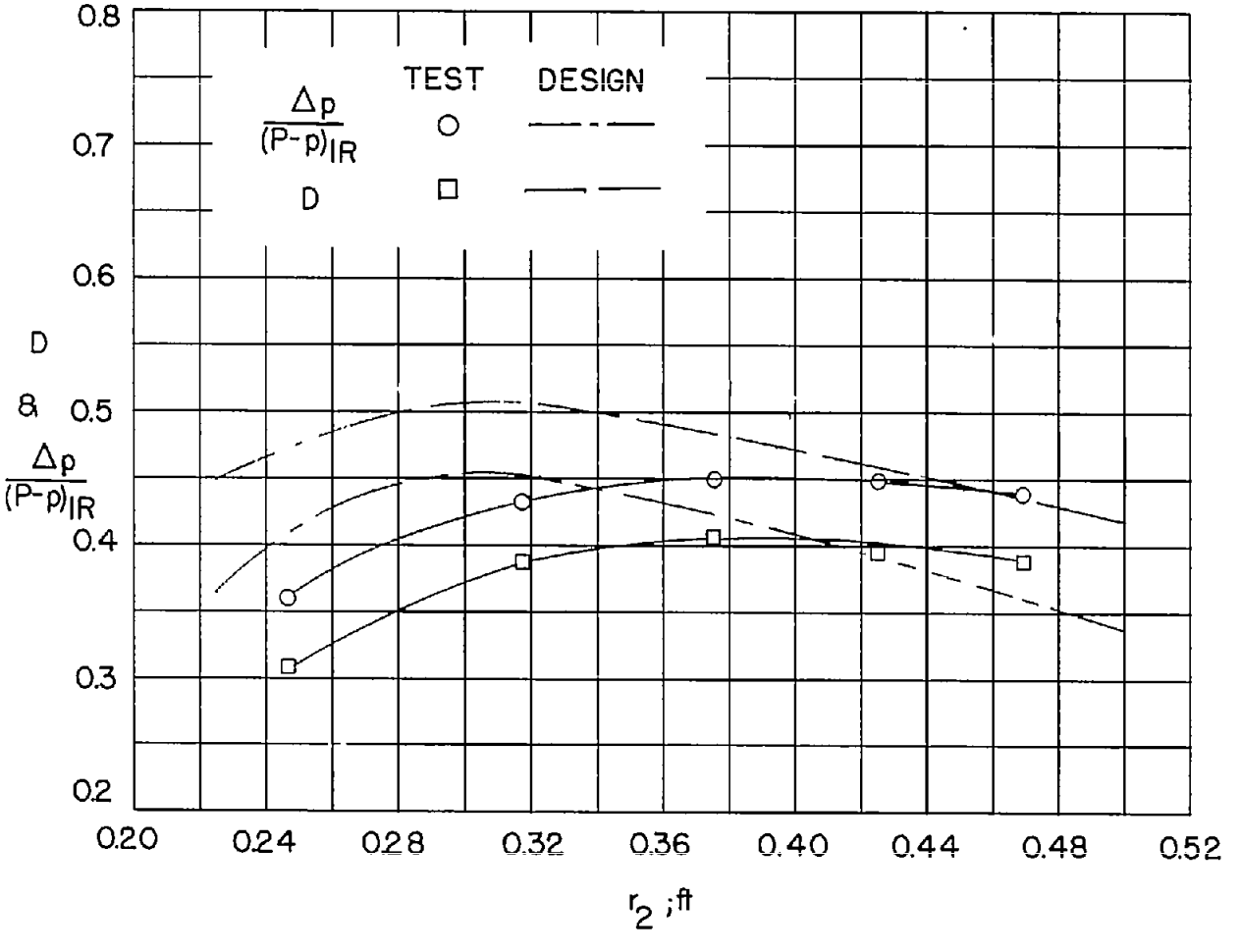

(i) Diffusion factor D and pressure-rise coefficient $\frac{\Delta p}{(P - p)_{1R}}$.

Figure 14.- Concluded.

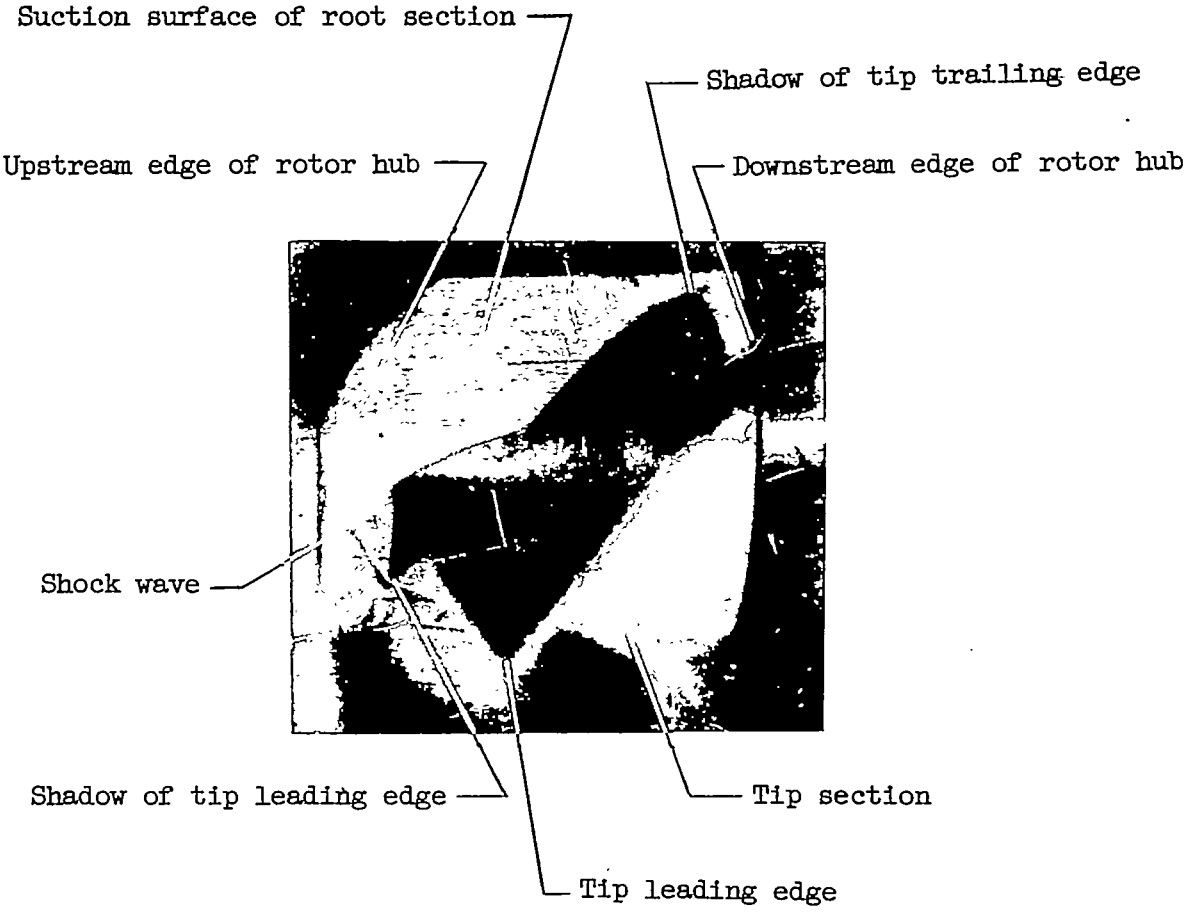

L-95884

Figure 15.- Typical shadowgraph photograph.

(a) 1.00 N_d

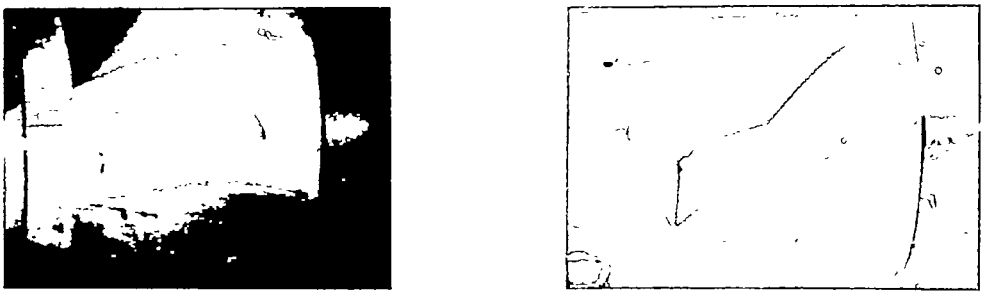

(b) 1.11 N_d

(c) 1.21 N_d

L-95885

Figure 16.- Typical shadowgraphs taken at three speeds at maximum flow.

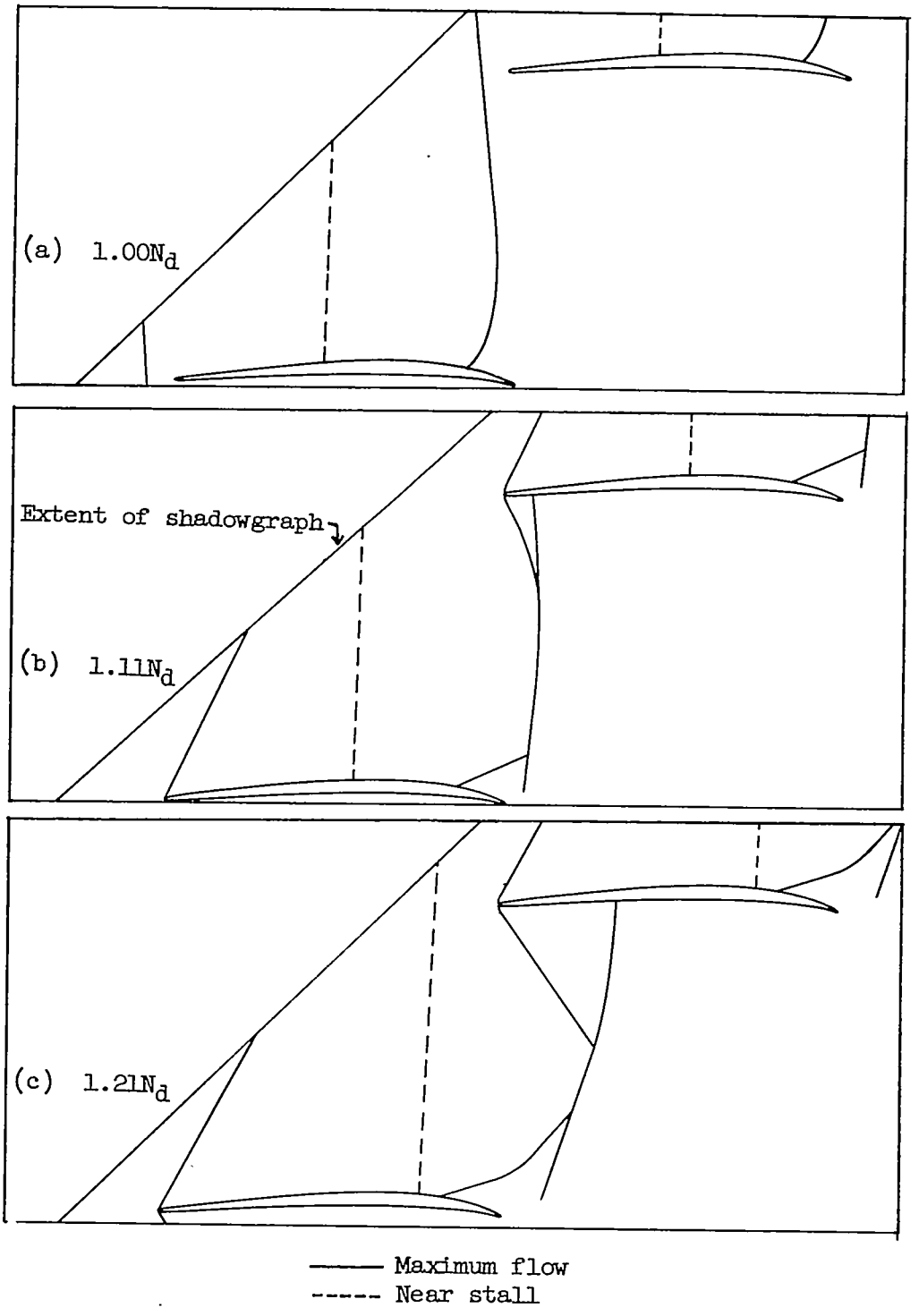

Figure 17.- Sketches of shock waves at the rotor tip at three speeds as determined by shadowgraphs. $\sigma = 0.75$; $\beta - \alpha = 46.4^{\circ}$.

A motion-picture film supplement, carrying the same classification as the report, is available on loan. Request will be filled in the order received. You will be notified of the approximate date scheduled.

The film (16 mm., 12 min., B&W, silent) shows the test rig and camera arrangement. Since the rotor blade moves approximately 0.3° between frames, about 150 frames are required to cover a complete passage. Because the condenser recharging time of the spark source is about 1 second, a lapse of approximately 100 to 140 revolutions exists between each pair of frames. Although the shock waves appear to be moving in these sequences, they are actually fixed relative to the blade. The first group of film sequences presents the open-throttle condition at three rotor speeds, as follows:

Sequence	Percent design speed	Inlet relative Mach number	Specific weight flow, lb/sec/sq ft
1	100	1.06	37.4
2	110	1.17	39.0
3	120	1.27	40.0

The second group of four sequences shows the effect of varying weight flow from open throttle to near surge at design speed, as follows:

Sequence	Specific weight flow, lb/sec/sq ft	Tip angle of attack, deg
1	37.4	7.1
2	36.5	8.4
3	34.6	10.5
4	33.0	12.6

NOTE: It will expedite the handling of requests for this classified film if application for the loan is made by the individual to whom this copy of the report was issued. In line with established policy, classified material is sent only to previously designated individuals. Your cooperation in this regard will be appreciated.

CUT

Date_____

Please send, on loan, copy of film supplement to RM L56K23

_____

Name of organization

_____

Street number

_____

City and State

Attention:* Mr._____

Title_____

*To whom copy No. ___ of the RM was issued

Place
stamp
here

Chief, Division of Research Information
National Advisory Committee for Aeronautics
1512 H Street, N. W.
Washington 25, D. C.